Photoemission Electron Microscopy and Atomic Force Microscopy of Phase-Separated Langmuir-Blodgett Monolayer Thin Films

A Thesis Submitted to the College of

Graduate Studies and Research

in Partial Fulfillment of the Requirements

for the Degree of Master of Science

in the Department of Chemistry

University of Saskatchewan

Saskatoon

By

Stephen Lynd Christensen

Permission to Use

In presenting this thesis in partial fulfillment of the requirements for a postgraduate degree from the University of Saskatchewan, I agree that the Libraries of this University may make it freely available for inspection. I further agree that permission for copying of this thesis in any manner, in whole or in part, for scholarly purposes may be granted by Professors M.F. Paige and S.G. Urquhart who supervised my thesis work or, in their absence, by the Head of the Department of Chemistry or the Dean of the College of Graduate Studies and Research. It is understood that any copying or publication or use of this thesis or parts thereof for financial gain shall not be allowed without my written permission. It is also understood that due recognition shall be given to me and to the University of Saskatchewan in any scholarly use that may be made of any material in my thesis.

Request for permission to copy or to make other use of material in this thesis in whole or in part should be addressed to:

The Head
Department of Chemistry
University of Saskatchewan
Saskatoon, Saskatchewan
Canada S7N 5C9

Abstract

Langmuir-Blodgett (LB) organic monomolecular (monolayer) films containing fatty acids and their perfluorinated counterparts separate into phases under certain conditions. These perfluorinated surfactant containing mixed-phase systems have been shown to exhibit many favourable attributes in comparison to non-perfluorinated surfactant monolayers. In this thesis project, two of these films were investigated. One film is a 2:1 ratio mixture of arachidic acid ($C_{19}H_{39}COOH$ – AA) to perfluorotetradecanoic acid ($C_{13}F_{27}COOH$ – PA), which phase-separates into hexagonal domains ~6 μm large (2:1 ratio of AA to PA – 2AA1PA). The other film is a 2:1 mixture of stearic acid ($C_{17}H_{35}COOH$ - SA) to PA, which phase-separates into linear domains ~300 nm wide (2:1 ratio of SA to PA – 2SA1PA).

Through the use of atomic force microscopy (AFM), and various synchrotron photoemission electron microscopy-based (PEEM) techniques, the films were characterized. As properties such as molecular organization, and dispersion of the molecules in the film, affect film function, it is necessary to use a variety of techniques to better understand order and composition in the films.

First, the well-known and previously-studied film, 2AA1PA, was used to better understand contrast mechanisms in the energy filtered x-ray photoemission electron microscope (X-PEEM) at the CLS. Through the use of techniques such as secondary electron emission microscopy (SEEM), ultraviolet photoelectron spectroscopy (UPS), and x-ray linear dichroism microscopy (XLDM), the effects of secondary electrons, valence character, and polarization dependence were studied so as to better understand their contribution to contrast in energy-filtered PEEM-based spectromicroscopy.

Second, the composition and organization of a novel system (2SA1PA), was characterized using traditional near-edge x-ray absorption fine-structure (NEXAFS) spectroscopy. As the size of the domains in the 2SA1PA system are below the spatial resolution limit of PEEM spectromicroscopy, methods involving selective phase

dissolution, and spectrum subtraction, were used to acquire phase composition and molecular order information.

The high lateral and vertical spatial resolution of AFM allowed physical imaging and confirmation of sample structure, as well as very accurate domain height determination. X-PEEM supplements this with chemical sensitivity using high spatial resolution spectromicroscopy. Therefore, using AFM and X-PEEM as complimentary techniques, it is possible to physically and chemically characterize phase-separated monolayer films.

Acknowledgements

I would like to thank my supervisors, Professor Stephen G. Urquhart and Professor Matthew F. Paige. Their constant leadership, guidance, and support enabled me to learn much; as well as piquing my interest in synchrotron-based physical chemistry. Their advice and education will be great assets for my future career in chemistry.

My advisory committee: Dr. L. Burgess, Dr. M.F. Paige, and Dr. S.G. Urquhart, deserve credit for their advice and constructive criticism throughout my project.

The members of the Paige and Urquhart labs were very helpful and I am sincerely grateful to them. They include Dr. Brian Haines, Dr. Uday Lanke, Dr. Edwige Otero, Dr. Shatha Qaqish, Danielle Covelli, Jahangir Valiani, Dr. Juxia Fu, Mitra Masnadi, and Shirin Behyan.

I wish to thank the University of Saskatchewan, the Department of Chemistry and its staff, the helpful staff at the Canadian Light Source, Dr. Chithra Karunakaran, Dr. Yongfeng Hu, and Dr. Lucia Zuin, and the Advanced Light Source, Dr. Andrew Doran and Dr. Andreas Scholl. These people provided valuable aid and expertise to my project.

Finally, I am extremely grateful to my loving family: my wife Morgan, my parents Brian and Helen, and my sister Amanda. If not for their encouragement, wisdom, and support, I could have never achieved my goals.

Table of Contents

Table of Figures

Chapter 1

Chapter 2

Chapter 3

Chapter 4

List of Abbreviations

AA	Arachidic Acid
AFM	Atomic Force Microscopy
ALS	Advanced Light Source
CaPeRS	Canadian Photoemission Research Spectromicroscope
CLS	Canadian Light Source
EPU	Elliptical Polarizing Undulator
EMR	Electromagnetic Radiation
HOMO	Highest Occupied Molecular Orbital
IP	Ionization Potential
IR	Infrared
LD	Linear Dichroism
LB	Langmuir-Blodgett
NEXAFS	Near-Edge X-ray Absorption Fine Structure
PA	Perfluorotetradecanoic Acid
PEEM	Photoemission Electron Microscopy
PEEM-2	PEEM-2 Microscope, ALS
PES	Photoelectron Spectroscopy
PTFE	Poly (tetrafluoroethylene)
SA	Stearic Acid
SE	Secondary Electron
SFM	Scanning Force Microscopy
SEEM	Secondary Electron Emission Microscopy

SM	Spectromicroscopy beamline, CLS
STXM	Scanning Transmission X-ray Microscopy
TDM	Transition Dipole Moment
THF	Tetrahydrofuran
UV	Ultraviolet
VLS-PGM	Variable Line Spacing – Plane Grating Monochromator, CLS
VUV	Vacuum Ultraviolet
XANES	X-ray Absorption Near-Edge Structure
XAS	X-ray Absorption Spectroscopy
XLDM	X-ray Linear Dichroism Microscopy
X-PEEM	X-ray Photoemission Electron Microscope

Chapter 1 Introduction

Surfactant monolayer containing a perfluorinated component exhibit interesting characteristics. The addition of a small quantity of a perfluorinated fatty acid to a surfactant film drastically reduces the monolayer's coefficient of friction, increases the chemical and physical inertness of the film, and generally improves film stability, impeding degradation[1,2,3]. These properties make these films useful in many fields, from being used as industrial lubricants[2,4], to medical applications, such as cardiac stent coatings[5].

Amphiphilic molecules, consisting of a polar "head" group and a non-polar "tail" group align on interfaces (i.e. air-water, water-oil, etc.), organized in such a manner that the head group imbeds itself in the polar region and the tail group orients so as to reduce contact with the polar solvent[6,7]. This means that amphiphilic molecules align on the air-water surface. The perfluorinated amphiphile behaves differently. As with the protonated surfactant, the polar head group imbeds itself in the polar solvent[6,7], however weak van der Waals interactions between the perfluorinated molecules mean the molecules manifest both hydrophobic and lipophobic properties, as opposed to the solely hydrophobic properties of their protonated counterparts[6,7]. While they orient in the same normal manner as protonated surfactants, there is a tendency to minimize contact with the non-polar end-groups of the protonated molecules. It is therefore common for mixtures of protonated and perfluorinated surfactants to phase-separate, forming domains on the air-water interface[6,7].

Because of the surface topography that forms in these phase-separated multi-component films, characterization of film composition and domain identity is of interest. The molecules comprising the films give order to the system. It is therefore also important to determine the orientation of the molecules in these films. If the molecules lie at an angle to the surface, it is of interest whether this alignment is isotropic or anisotropic.

Synchrotron-based x-ray spectromicroscopy is ideal to characterize both the domain composition and molecular orientation in mixed-phase LB film

systems[8,9,10,11]. Using x-ray photoemission electron microscopes (X-PEEM) at high-intensity monochromatic x-ray sources such as the Canadian Lightsource (CLS) in Saskatoon, Saskatchewan, and the Advanced Light Source (ALS) in Berkeley, California, simultaneous microscopy and spectroscopy of a sample (spectromicroscopy) is possible.

The PEEM microscope at the CLS is the Canadian Photoelectron Research Spectromicroscope (CaPeRS), and it is fitted with an imaging energy analyzer. This analyzer provides the ability to probe the workfunction and valence character of the films through the use of photoemission spectroscopy[11]. NEXAFS spectroscopy using PEEM is a well-established surface-sensitive characterization method[10,11,12,13,14].

There are two primary objectives of this M.Sc. project: the use of well-characterized Langmuir-Blodgett monolayers to better-understand contrast mechanisms in the CaPeRS X-PEEM, and the characterization of less-understood Langmuir-Blodgett monolayers by well understood microscopic and spectromicroscopic methods. It is important to note that due to the small amount of sample, radiation damage is a problem, and they become very difficult systems to study.

Well-understood films consisting of domains less than 6 μm long have previously been characterized using AFM height measurements and selective dissolution studies to determine domain composition[15]. These films, and the size of their domains, make them excellent model systems to better understand the contrast mechanisms involved with the CaPeRS X-PEEM. The effect of the spectromicroscope's imaging energy analyzer on the data collected of these films is not well understood. Since the films are well characterized, they can be used to better-understand the effectiveness of ultraviolet photoelectron spectroscopy (UPS) and secondary electron emission microscopy (SEEM) as molecular valence probing techniques in PEEM.

To accomplish the second goal, well known spectromicroscopy and atomic force microscopy techniques can be used to characterize novel phase-separated LB organic monolayer films, determining their composition. Using AFM, the sample's

surface topography is determined, as well as the physical characterization of domain height and organization[16]. NEXAFS spectromicroscopy allows the spectroscopic chemical characterization of the individual domains, and x-ray linear dichroism microscopy (XLDM) determines the molecular orientation[17,18]. Therefore well-understood techniques were used to characterize a poorly-understood phase-separated LB system.

1.1 Langmuir-Blodgett (LB) Technique

Langmuir-Blodgett films were used in these experiments because of the reproducibility and consistency with which they create the phase-separated 2AA1PA and 2SA1PA systems. The 2AA1PA system was used to better-understand PEEM contrast mechanisms, and the interesting physical chemistry of the 2SA1PA system, became better-understood through well-established PEEM-NEXAFS techniques.

When a small amount of surfactant is dispersed on the air-water interface, it forms a monomolecular (monolayer) film (figure 1.1). These films are known as Langmuir films after Irving Langmuir, the Nobel Prize winning scientist who pioneered monolayer and interfacial chemistry[6,7].

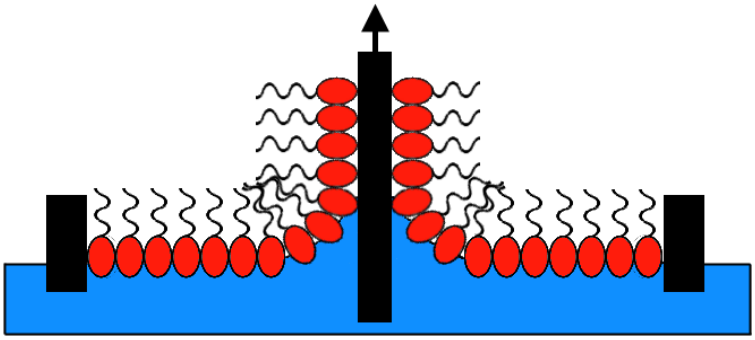

Figure 1.1 - Schematic illustration of Langmuir-Blodgett technique for deposition of amphiphilic layers.

A Langmuir-Blodgett monolayer is formed when a substrate is drawn through the film present at the air-water interface. This technique is named after Katherine Blodgett, who applied deposition of Langmuir monolayers extensively in her

research[6,7]. Langmuir-Blodgett films are extensively used, especially for the study of bio-films and lubricants. Bilayer LB films of phospholipids mimic cell membranes, making them useful for biological and pharmaceutical study, while LB systems with low friction coefficients make ideal industrial lubricants[2,4,6,7].

1.1.1 Surface Pressure-Area Isotherm

Useful thermodynamic information about amphilic systems can be obtained from a surface pressure-area isotherm. In these measurements, amphiphilic molecules containing both polar and non-polar regions are dispersed on a phase interface such as that between air and water, in a poly(tetrafluoroethylene) (PTFE) trough (figure 1.1). The surfactant molecules then spread on this surface, minimizing interactions with each other, creating a dispersed monolayer. Two barriers are slowly moved towards each other, compressing the film, reducing the available mean molecular area, and therefore increasing the surface pressure. Surface pressure (represented by the symbol Π) is the difference in surface tension between that of the water subphase (γ_{water}), and that of the film-covered surface ($\gamma_{surfactant}$)[6,7], such that:

$$\Pi = \gamma_{water} - \gamma_{surfactant} \qquad (1.1)$$

Since molecular films reduce the surface tension of the pure subphase, the surface pressure increases as the surface tension of the film-covered surface decreases[6,7]. This relationship is referred to as a surface pressure-area isotherm and provides thermodynamic information about the monolayer.

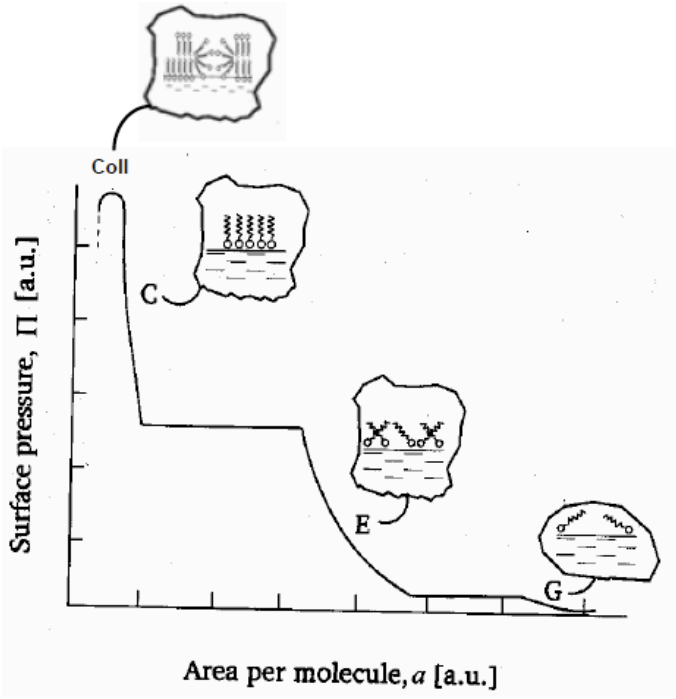

Figure 1.2 - Illustration of a surface pressure-area isotherm, showing surface pressure change from gas-like to solid-like phases. (figure adapted from M.C. Petty, 1996)[6]

A surface pressure-area isotherm is a graphical means of representing change in surface pressure as the mean molecular area of the surfactant molecules is being reduced. When compressing the LB film, the surfactant monolayer, surface pressure-area isotherm exhibits changes that represent the two-dimensional phase character of the monolayer (figure 1.2). When the film is very diffuse, the molecules act in a gas-like manner (G), remaining at the interface, but without order or orientation. In this state there is little interaction between the molecules. As the mean molecular area decreases, the monolayer becomes more ordered and is referred to as a liquid-like state (E). This phase is sometimes referred to as the expanded monolayer phase[6].

The next phase, the solid-like state (C), is where the monolayer takes on a more rigid form. Since the mean molecular area is so small (generally the diameter of the molecule), to reduce interaction with other molecules the amphiphile molecules adopt more vertical orientations.

The collapse stage (Coll) in the surface pressure-area isotherm occurs when it is not possible to compress the film anymore; it has reached its maximum surface

pressure. Any further compression results in collapse of the film. Collapse occurs when it is more thermodynamically favourable for the molecules to leave the air-water interface and form local double-layer regions[6,7]. This is represented by a reduction in surface pressure. The plateau regions of the surface pressure-area isotherm are regions of coexistence.

1.1.2 Systems Investigated in the Thesis

Two phase-separated mixtures were used for these experiments. The first mixture (2AA1PA) was comprised of a 2:1 ratio of arachidic acid (AA) to perfluorotetradecanoic acid (PA) (2AA1PA). These surfactants phase-separate into micron-sized discontinuous hexagonal domains of AA, surrounded by a continuous domain of PA[11,15]. The 2AA1PA system was chosen because of its reproducible hexagonal domain formation of an ideal size for PEEM microscopy. As the system is well-understood, it was used to explore and better understand the different energy-filtered X-PEEM contrast mechanisms. The second mixture, was comprised of a 2:1 ratio of stearic acid (SA) to perfluorotetradecanoic acid (PA) (2SA1PA)[19]. The 2SA1PA system was used as the linear domains are reproducible, yet too small to be spatially resolved by PEEM (having a spatial resolution limit of ~30 nm). Well-understood PEEM-based NEXAFS techniques were used to characterize this relatively unknown system.

1.1.3 Helicity of Saturated Perfluorinated Molecules

Perfluorotetradecanoic acid, like other perfluoroalkanes or perfluorocarboxylic acids, adopts a helical conformation. Jang et al. determined using empirical data, and ab-initio calculations that the electrostatic interactions between the fluorine atoms establishes the helical conformation[20,21]. Figure 1.3 below depicts the helix along the carbon backbone of the PA molecule. The model was produced using the Spartan ’06 molecular modeling suite; the conformation being determined using geometry optimization of the Hartree-Fock 6-31G* level of theory. This helical conformation means that the x-ray absorption induced transition dipole moments (TDM) from the different carbon atoms are rotationally averaged,

therefore affecting polarization-dependent measurements; to what extent is discussed in section 1.4.2.

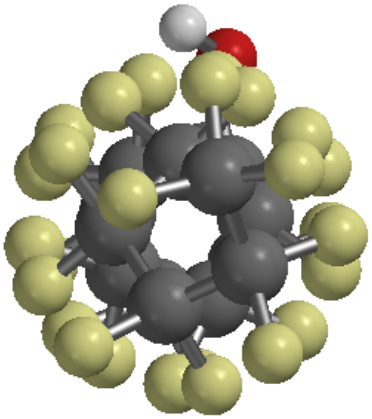

Figure 1.3 - Model of perfluorotetradecanoic acid in vacuum, depicting helical conformation due to electrostatic repulsion of the fluorine atoms. Molecular modeling calculations were performed using the HF 6-31G* geometry optimization.

1.2 Atomic Force Microscopy

Atomic force microscopy was the primary characterization method used to characterize the surface topography of the monolayer films. The high vertical and lateral resolution of this scanning force microsocopy (SFM) made sub-nanometer variations in sample topography measureable, while minimizing damage to the sample.

AFM is a high-resolution scanning probe imaging technique, wherein a cantilever with a Si_3N_4 tip is drawn across the surface of a sample. Small topographical features cause deflection of the cantilever, which in turn changes the position of a laser that is reflected off the back of the cantilever. Changes in position of the laser are recorded by a photodiode. The technique is capable of molecular resolution, and simultaneous measurements of height, tip deflection, and tip-surface interaction friction. The sensitivity of the instrument used allows for a lateral resolution of a few nanometers, while the vertical resolution is sub-nanometer.

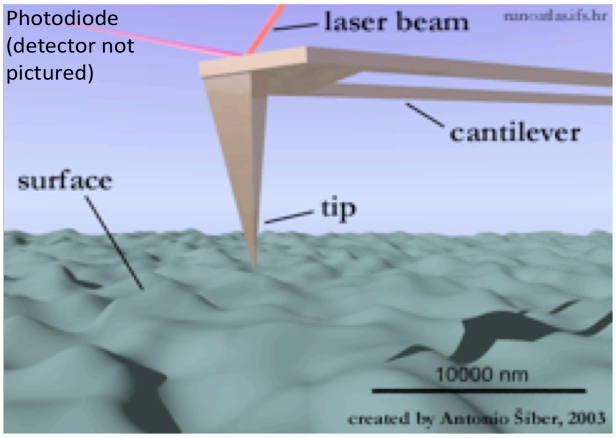

Figure 1.4 - Diagram of atomic force microscope (AFM).
(Figure adapted from A. Saber, 2003)[22]

1.3 Photoemission Electron Microscopy (PEEM)

PEEM is capable of full-field imaging of surface areas from 1-80 μm in diameter. This technique relies on imaging photo-ejected electrons. To obtain chemically sensitive information, PEEM makes use of NEXAFS spectroscopy. In NEXAFS spectroscopy, electrons are excited from core orbitals to unoccupied orbitals, or ionized into the continuum. The energies at which these excitations occur are sensitive to chemical state and bonding and therefore have some elemental and chemical specificity. Because of this ability, the PEEM is a valuable tool for mapping surface regions and giving insight into surface composition.

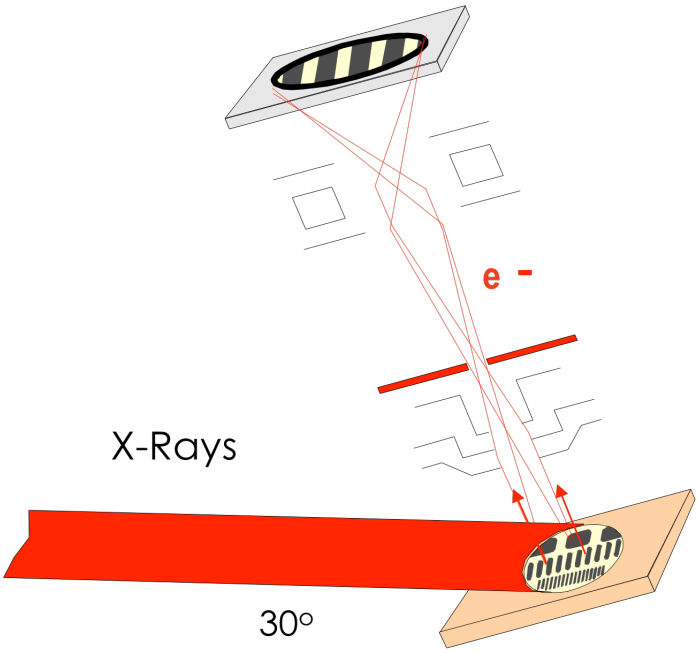

Figure 1.5 - Diagram of PEEM with lens system. (Figure adapted from A. Scholl)

As shown in figure 1.5, incident photons (x-rays or VUV) impinge on and are absorbed by the sample. The ejected primary photoelectrons propagate through the sample and scattering in-elastically, creating secondary electrons. Only those primary and secondary electrons generated near to the surface retain enough kinetic energy to overcome the surface workfunction, and are ejected from the sample surface. Workfunction (φ) is the energy required to eject an electron from inside the material, to a point just outside the material (continuum). These ejected electrons are subsequently accelerated and focused by an objective lens. A series of magnetic and electrostatic lenses focus and magnify the photoelectron image onto a multichannel plate, where the signal is intensified and projected onto a phosphor screen. The phosphor screen is positioned in front of a CCD camera, and each photoelectron-phosphor event that creates visible light is detected by the CCD camera. The more photoelectrons emitted, the more counts the CCD receives, and the greater the measured intensity for each CCD pixel. This means that when a sample strongly absorbs the incident photons, the brighter the measured CCD signal will be.

A benefit to electron-yield is the inherent surface sensitivity, as only electrons with the kinetic energy to overcome the workfunction are measured. For electron

kinetic energies ~50-100 eV, this means an escape depth of ~ 5 nm, and a shallower incidence angle can increase the signal coming from this sample volume[30].

Experiments were conducted on a few beamlines, depending on when experiment time was available, and what experiments were to be run. All synchrotron-based experiments were performed using an X-PEEM.

For this research, two PEEM microscopes were used: one was the Canadian Photoelectron Research Spectromicroscope (CaPeRS)[11] located on both the Variable Line-Spacing Plane-Grating Monochromator (VLS PGM)[23] beamline, and the Spectromicroscopy (SM)[24] beamline at the Canadian Light Source (CLS – Saskatoon, SK, CA), and the other was the PEEM-2, located permanently on the Photoemission Microscopy beamline (7.3.1.1)[25] at the Advanced Light Source (ALS – Berkeley, CA, USA).

One major difference between the CaPeRS PEEM and the PEEM-2 is the presence of an energy filter on the CaPeRS X-PEEM.

1.3.1 Advantages of Energy-Filtered PEEM

A major advantage of the CaPeRS PEEM over the PEEM-2 is the presence of an energy-filter. This filtering of electrons by their kinetic energy enables the acquisition of SEEM XPS, and UPS spectra. Chapter 3 discusses spatially resolved UPS experiments of phase-separated 2AA1PA films. The ability of the energy-filter to reduce chromatic aberrations means a better spatial resolution. The energy-filter also means the PEEM is capable of making XPS, UPS, and SEEM measurements using a low-dose technique called dispersion mode, which is discussed in depth in section 3.5.

Although difficult to use with organic monolayer films, there are many examples where the use of an energy-filter has been advantageous[26], such as determining the orientation in a self-assembled monolayer semi-fluorinated surfactant system on SiO_x by XLDM-NEXAFS[27], and radiation damage studies of Si_xN_y interface on Si(111) using XPS[28].

1.3.2 Challenges of Energy-Filtered PEEM

As the instrument title suggests, the energy-filter is capable of filtering electrons used for imaging, based on their kinetic energy. This reduces the electrons counted by the CCD camera. The increased radiation damage, which comes from longer dwells for better statistics, is not a problem for metals, but is detrimental for organic samples. As the energy filter accepts a narrow energy range of electrons, image contrast can be distorted.

Energy-filtered PEEM is able to probe workfunction differences more directly than conventional PEEM, and therefore more sensitive to surface contamination when dealing with organic monolayer films. Because of the narrow band-pass of accepted electron kinetic energies accepted by the energy-filter, as rapid change to the distribution of electron kinetic energies with photo-desorption of surface contaminants, causes spectra to vary with changes in workfunction over the course of a few seconds. Effects such as photodeposition and water desorption may significantly change the workfunction of the sample, leading to changes in secondary electron emission.

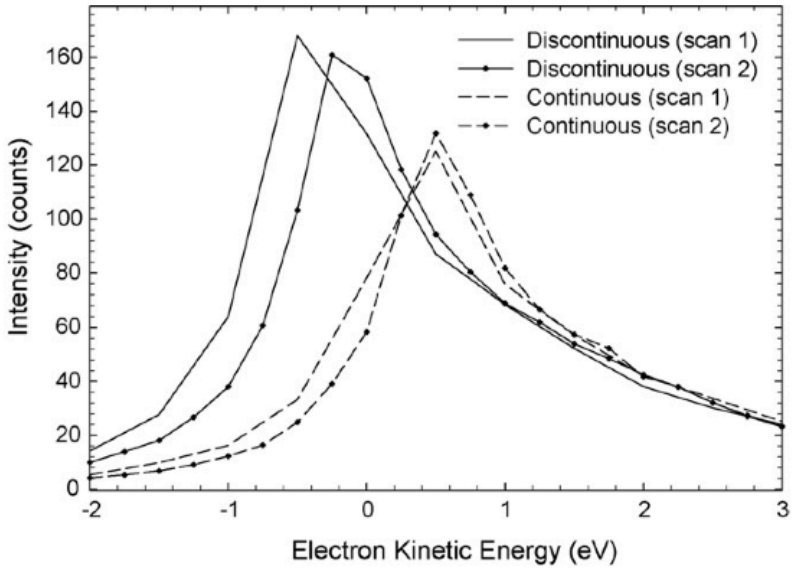

Figure 1.6 – Secondary electron emission microscopy of 2AA1PA LB system discontinuous and continuous domains[11]

As shown in figure 1.6, the secondary electron (SE) band can therefore change with the band-pass of the energy-filter. Over or under-sampling of phases can occur as different molecules have different workfunctions, and can therefore yield non-quantitative results.

1.3.3 PEEM Contrast Mechanisms

In PEEM spectromicroscopy, contrast is due to workfunction effects, surface topography, and photoabsorption. It is the contrast due to NEXAFS features which enables chemical characterization of the sample surface.

The x-ray absorption cross-section is primarily responsible for the intensity observed. The absorption cross section is the probability of photon absorption; of one incident photon inducing the photoabsorption or electron photoemission. This probability decreases with increasing energy, as the x-ray absorption coefficient, μ, is given by:

$$\mu = \frac{\rho Z^4}{AE^3} \tag{1.2}$$

where ρ is the density, Z is the atomic number, A is the atomic mass, and E is the incident x-ray energy. This is the reason for decay of the absorption cross-section as a function of energy, meaning that the higher the incident energy, the less photo-ionization will occur, and there is a corresponding reduction in signal and contrast.

An absorption edge cross-section occurs at the ionization potential for a core electron. There is a weaker signal below the edge (from valence electron photoionization) Discrete pre-edge absorption features are present below the edge. The spectrum becomes more intense at the edge. Continuum transitions are superimposed on the photoionization crosssection above the ionization edge. This is explained in more detail in section 1.4.

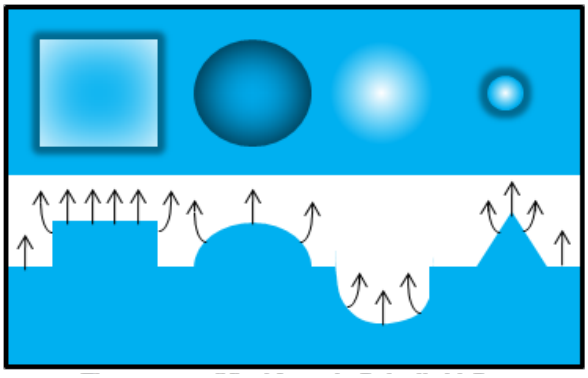

Figure 1.7 - Contrast map of intensity change with variations to surface topography. (Figure adapted fro A. Scholl)

Surface topography also has an effect on the photoemission intensity of the sample, as electrons leave the surface with different paths depending on the sample's topography. This effect is illustrated in figure 1.7. If a feature is sharp, field emission can occur and the feature can appear extremely bright. Electrons escaping from a convex feature will appear darker than their flat surroundings, while electrons escaping from a concave feature will appear brighter than their flat surroundings. Shadowing occurs when a feature blocks the incident photons, casting a shadow on the surface. Since the photons cannot obtain a direct path to the surface, the only signal from these areas will be from secondary electron processes originating from outside the shadow region.

Contrast is also affected greatly by the x-ray absorption spectrum of the surface. When core electrons are excited by x-ray absorption, an Auger decay process will lead to subsequent photoelectron emission. This and inelastic scattering provides a secondary electron emission signal proportional to the x-ray absorption cross-section. X-ray linear dichroism studies[17,18] have demonstrated that intensity and contrast, can depend on the angle of the molecule's electronic transition with respect to the x-ray electric field polarization vector.

1.4 Photoabsorption Contrast

1.4.1 Near-Edge X-Ray Absorption Fine-Structure (NEXAFS) Spectroscopy

X-ray spectroscopy features occurring within ~30 eV before and after the absorption edge are labeled as NEXAFS features. When a photon excites a core electron with equal or greater energy than the binding energy of the core electron, the electron is photo-ejected from the atom or molecule. The energy required to photo-eject an electron, therefore ionizing the atom or molecule, is referred to as the ionization potential (IP), and is described by:

$$E_B = h\nu - E_k - \varphi \tag{1.3}$$

where E_B is the binding energy, $h\nu$ is the incident photon energy, E_k is the kinetic energy, and φ is the workfunction of the surface. NEXAFS spectroscopy involves the excitation of core electrons to unoccupied orbitals or bands (see Figure 1.9) as well as photoionization. Small differences in the binding energies of core electrons (e.g. when bound to electron donating or withdrawing groups) or the energy of valence orbitals (from bonding or conformation) will give rise to fine-structure, making NEXAFS spectroscopy sensitive to chemical composition. Molecular orientation can also be studied through angle dependent NEXAFS.

As seen in figure 1.9, if the energy of the incident photon corresponds to that of a specific core → valence transition (eg. C 1s→σ*, O 1s→π*, or C 1s→ Rydberg states), excitation will occur. Subsequent Auger decay process gives rise to an emitted electron[29].

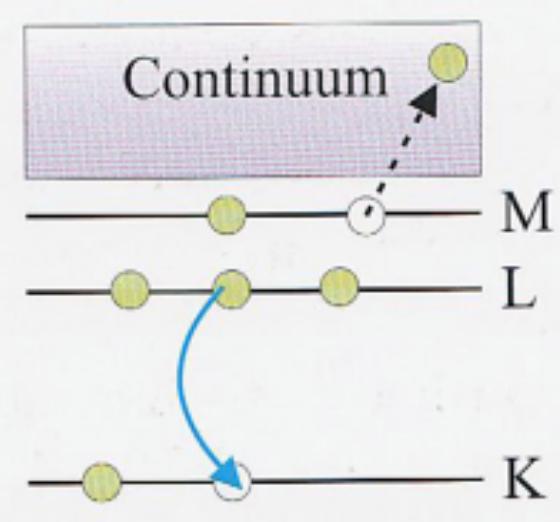

Figure 1.8 – Illustration of Auger decay process in x-ray spectroscopy. (Figure adapted from J. Als-Nielsen and D. McMorrow, 2001)[29]

The NEXAFS of elements with low atomic number is primarily obtained by electron-yield measurements, as the fluorescence yield is minimal for low-Z elements. Non-radiative Auger processes dominate at energies <2000 eV, as where radiative processes are more probable at higher energies.

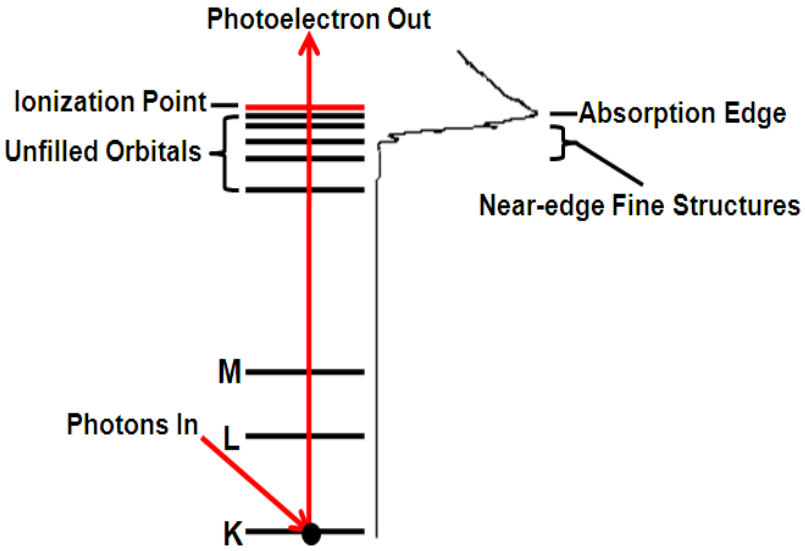

Figure 1.9 - Diagram depicting photoemission mechanism contributing to NEXAFS spectral features.

With organic molecules, such as the surfactants being studied, excitation of core electrons to unoccupied anti-bonding molecular orbitals (depicted in figure 1.9) results in spectral features characteristic of chemical environments. This results in systematic shifts in binding energy with chemical bonding. Since fluorine is more electronegative, when bonded to carbon, the binding energies of the carbon atom electrons are shifted to a higher binding energy. A good example of binding energy dependence on functional group environment is shown in figure 1.10 below. Polyethylene (PE)[31] and polytetrafluoroethylene (PTFE)[32] demonstrate that differences in molecular functional environment significantly affect spectral energy shifts.

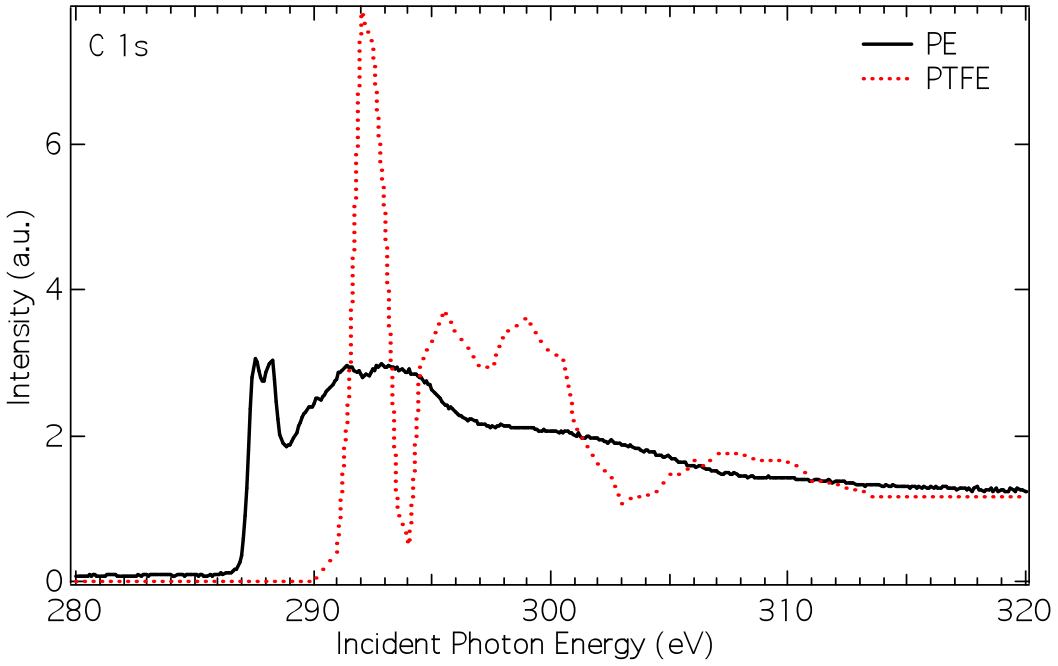

Figure 1.10 – Differences in spectral features of polyethylene on Si[31] and polytetrafluoroethylene on gold[32] with changes to molecular environment. (Figure adapted from O. Dhez, H. Ade, and S.G. Urquhart (PE), and L. Gamble, B. Ravel, D. Fischer, and D. Castner (PTFE))

1.4.2 Linear Dichroism (LD-NEXAFS) and X-ray Linear Dichroism Microscopy (XLDM)

LD-NEXAFS studies can be used to determine molecular orientation, using the preferential anisotropic absorption of linearly polarized electromagnetic radiation (EMR)[29]. LD-NEXAFS therefore exhibits angular dependence when the orientation of the electric field vector of EMR relative to the induced transition dipole moment of a molecule constructively interfere during photoabsorption.

Figure 1.11 - Diagram of electric field vector perpendicular to vector of propagation, and orthogonality of electric (E) and magnetic (H) fields for linear polarization. (Figure adapted from J. Als-Nielsen and D. McMorrow, 2001)[29]

As the two orthogonal components of EMR, the electric field vector (E) with amplitude ε and the magnetic field vector (H), propagate towards the sample with wave vector k, the E and H field vectors oscillate perpendicularly to the vector of propagation (figure 1.11)[29]. Excitation of core electrons to unoccupied states is the reaction of a system to an electric transition dipole moment perturbation[30].

The expectation value, μ_{if}, is defined by the initial and final wavefunction states when operated on by the electric dipole moment operator, μ:

$$\mu_{if} = \langle \psi_i | \mu | \psi_f \rangle \qquad (1.4)$$

Long-chain fatty acids or hydrocarbons are molecules consisting of a long single-bonded C-C chain (the "backbone"), with C-H groups running perpendicular to it every ~1.5Å[18].

$$I \propto \left| E \bullet \mu_{if} \right|^2 = \left| E \right|^2 \left| \mu_{if} \right|^2 \cos^2 \theta \qquad (1.5)$$

The angle between the E and μ_{if} vectors (θ), denotes that angular dependence can play a large role in feature intensity. The smaller the projection of E on the TDM, the lower the probability of TDM excitation, and a reduction in feature intensity will occur[30]. NEXAFS, therefore, can effectively measure molecular orientation, by the selective photo-excitation of certain in-plane TDMs by polarization of the incident electric field vector.

In figure 1.12 below[29], the EM radiation is propagating in a direction parallel to the C-C backbone, with the electric field oscillation vectors parallel to the C-H groups. The C1s$\rightarrow\sigma^*_{C\text{-}H}$ transition is therefore selectively excited, the evidence being the large $\sigma^*_{C\text{-}H}$ NEXAFS feature at 288 eV. When the opposite case is tried, and the direction of propagation is parallel to the C-H direction, the electric field vector oscillations are parallel to the carbon backbone, which is therefore preferentially exciting the C-C backbone. This is denoted by the much more intense C1s $\rightarrow$ $\sigma^*_{C\text{-}C}$ NEXAFS spectrum feature at 294 eV.

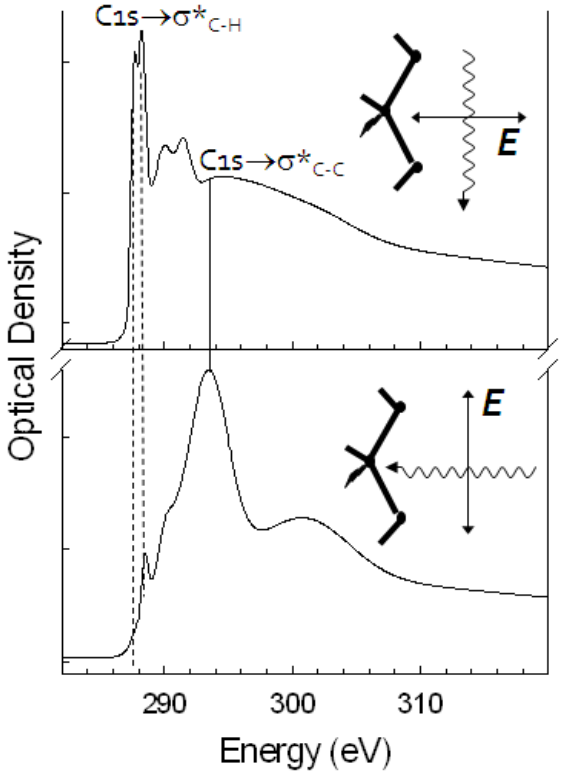

Figure 1.12 - C1s NEXAFS of hydrocarbon chain. In the top spectrum, the electric field (E) is exciting the C1s→$\sigma^*_{C\text{-}H}$ transition, and in the bottom, the C1s→$\sigma^*_{C\text{-}C}$ transition. (Figure adapted from J. Fu and S.G. Urquhart, 2005)[17]

X-ray linear dichroism microscopy (XLDM) images differences in feature intensity based on the angular dependence of the molecules. XLDM using X-PEEM allows the full-field imaging of entire regions with respect to their preferential absorption of polarized light. This means the imaging of molecular orientation over a field of view, allowing comparison of domains in the area. Therefore, angle-resolved NEXAFS spectroscopy can be used to study molecular orientation.

1.5 Photoemission

Photo-ionization of an atom or molecule occurs when photon absorption leads to electron emission:

$$h\nu + M \rightarrow M^+ + e^- \qquad (1.6)$$

where hν is the incident photon energy, M is the molecule or atom, M^+ is the resultant ion, and e^- is the photo-emitted electron. Energy is conserved in formula 1.6, as the incident photon energy is equal to the sum of the kinetic energy of the electron and the energy required to remove the electron from the atom or molecule (see equation 1.3).

Photoemission spectroscopy can be broken down into x-ray photoelectron spectroscopy (XPS), ultraviolet photoelectron spectroscopy (UPS), and secondary electron (SE) photoemission spectroscopy. XPS is not used in this research. UPS measures the photoemission of electrons from the valence band, while SE spectroscopy measures the low kinetic energy electrons generated by inelastic scattering in the sample.

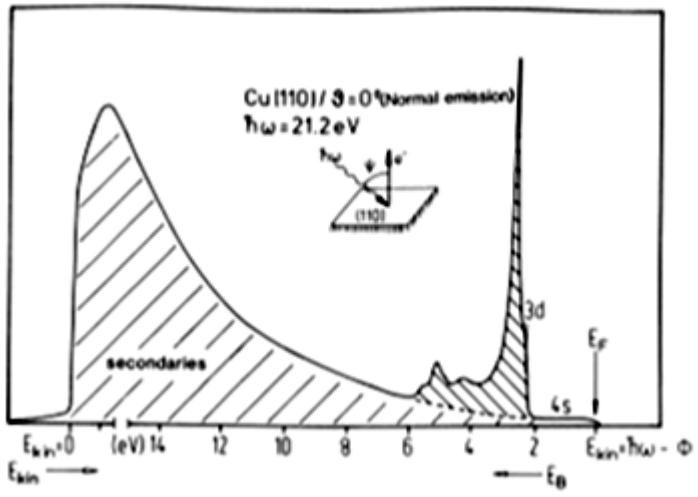

Figure 1.13 – Diagram of secondary electrons and valence electron emission from a Cu(110) surface at He Iα (21.2 eV). (Figure adapted from S. Hufner, 2003)[33]

The above figure 1.13 depicts an example of primary and secondary photoemission, based on the UV induced photoemission from a Cu(110) surface. The secondary electrons are distributed at low kinetic energies (E_K), and the valence features found at higher kinetic energies (or low binding energies (E_B) via equation 1.3). In figure 1.13, the UPS spectrum of Cu (110) can be interpreted as valence orbital energies in the conduction band using Koopman's Theorem (discussed in the

section 1.5.1). The secondary electron energies are created and escape with low E_K values. Figure 1.14 below demonstrates how secondary electrons escape the system with very low kinetic energy due to inelastic scattering as they propagate through the sample. As electrons interact inelastically with the system, they lose energy, and electrons of sufficient energy to overcome the workfunction are detected. This process is also known as the cascade of secondary electrons.

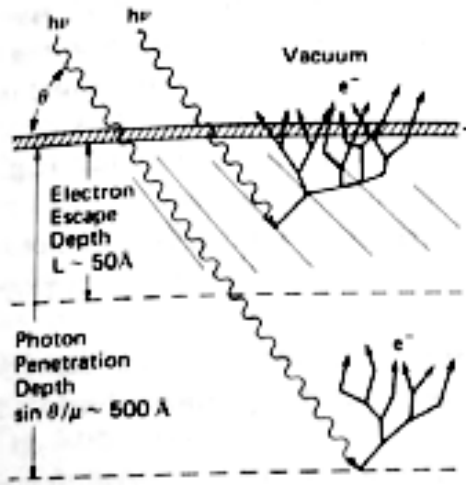

Figure 1.14 – Origin of secondary electrons demonstrated by propagation of photo-ejected electrons through sample, and kinetic energy loss by inelastic scatter of electrons. (Figure adapted from J. Stöhr, 2003)[30]

1.5.1 Ultraviolet Photoelectron Spectroscopy (UPS)

Photoelectron spectroscopy using vacuum-ultraviolet light (VUV) is referred to as UPS. This photoemission technique uses monochromatic VUV light to excite electrons out of weakly bound atomic or molecular orbital valence states[34].

UPS can supply information about valence and bonding character, band gap, workfunction effect, and vibronic states. Electrons excited from a molecular orbital mean they are provide information on valence character, as opposed to the chemical information obtained from core electrons[30,34].

Koopman's theorem, predicts that calculated orbital energies as equal but opposite to their ionization potential[34]:

$$I_j = -\varepsilon_j \quad (1.7)$$

where I_j is a specific ionization potential, and ε_j is its orbital energy.

Koopman's theorem uses electron orbital energies calculated by self-consistent field (SCF) theory. SCF is an iterative method, , which calculates the energy of each electron in the static field of the fixed nuclei and the frozen interaction of the remaining electrons[34]. ΔSCF measurements compare the energy of the system before ionization, and after the molecular cation is formed. This method accounts for relaxation of the remaining electrons, unlike the Koopman's theorem method. In both cases, the Born-Oppenheimer approximation is used, as changes to nuclear position occur at a much slower rate than that of the electrons, allowing treatment of the nucleus as a stationary entity[34].

1.5.2 Secondary Electron Emission Microscopy (SEEM)

SEEM is the imaging of a surface using the secondary electron emission peak. Electrons excited from deeper in the sample can lose kinetic energy to nearest neighbour electrons from the same or other molecules. These scattered electrons can still escape from the sample, if their kinetic energy is greater than the workfunction of the system (figure 1.15). These secondary electrons do not contain any relevant information about where they were emitted, but their energy distribution around low kinetic energy is sensitive to small workfunction changes, such as that caused by photo-desorption of water from the sample surface[35].

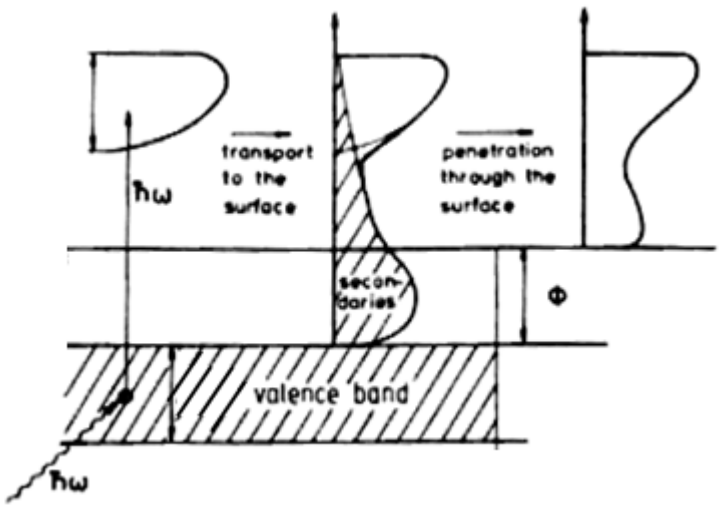

Figure 1.15 – Diagram of secondary electron process: 1) electrons are photoexcited, 2) propagation of secondary electrons to sample surface, and 3) electrons overcome workfunction and escape to vacuum. (Figure adapted from S. Hufner, 2003)[33]

SEEM is sensitive to the workfunction at the sample surface, as it is dependent on the low kinetic energy electrons which escape. Figure 1.16 below is referred to as the "universal curve", or mean-free path curve, demonstrating the average electron escape depth in solids as a function of electron kinetic energy. As depicted in figure 1.16, electrons with a kinetic energy of ~50-100 eV have an escape depth of ~5 Å. This means that there will be fewer and fewer secondary electrons with enough kinetic energy to overcome the system workfunction, the further into the sample the electron cascade processes occur (see figure 1.14 to visualize the cascade process).

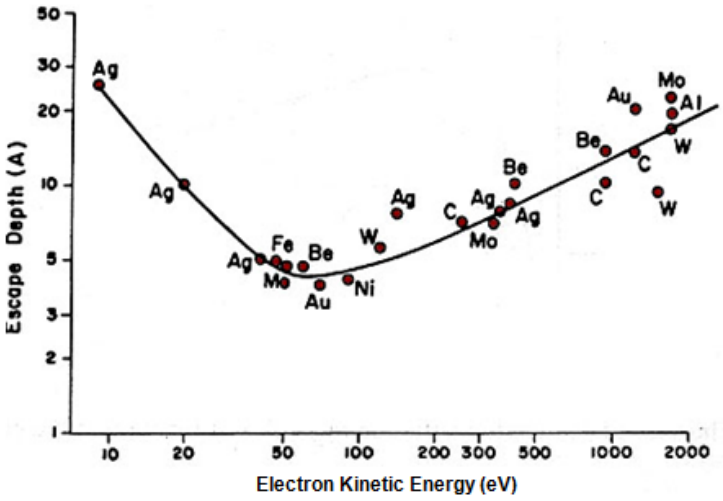

Figure 1.16 – Mean free path diagram depicting escape depth vs. electron kinetic energy. (Figure adapted from J.B. Hudson, 1992)[36]

Spectromicroscopy based on measurement of the secondary electron emission is known as secondary electron emission microscopy (SEEM). Figure 1.16 demonstrates that electrons with certain kinetic energies, created via secondary processes, emit from a certain averaged depth. SEEM is useful in determining effects caused by phase-mixing and surface topography, such as the difference in workfunction of the phases in the 2AA1PA system, or changes in workfunction as water desorbs from the sample surface in vacuum.

1.6 Synchrotron Radiation

X-PEEM NEXAFS and UPS spectromicroscopy experiments require highly collimated, tunable and monochromatic light. A synchrotron light source is needed for these types of experiments. Synchrotron facilities emit radiation at each bending magnet or insertion device (figure 1.17). This light is bright, highly monochromated, and can have controlled polarization.

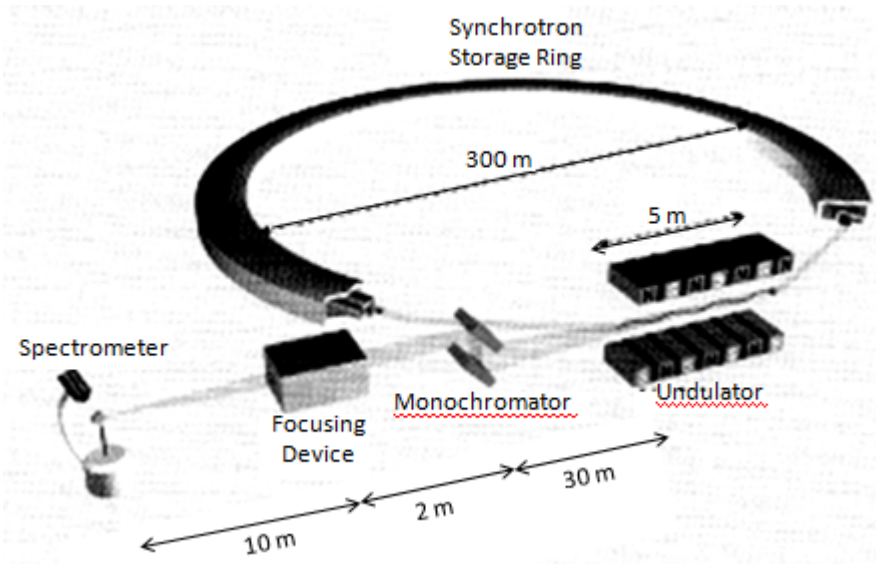

Figure 1.17 - General diagram of a synchrotron radiation facility, with insertion device, monochromator, and endstation. (Figure adapted from J. Als-Nielsen and D. McMorrow, 2001)[29]

1.6.1 Spectromicroscopy (SM) Beamline

The Spectromicroscopy (SM) beamline is located at the CLS synchrotron[24,37]. It is the beamline to which the CaPeRS X-PEEM is permanently attached. The SM beamline uses an Apple II elliptically polarizing undulator (EPU), capable of providing linear polarization with inclined azimuthal orientation over 180° linear, and left and right circular polarization. The beamline uses a plane-grating monochromator, and is capable of producing 150 eV to 2000 eV photons[24,37]. Initial NEXAFS experiments, as well as SEEM experiments were carried out on this beamline. This beamline is a very intense source of x-rays, and proper measures (shutters, detuning of undulator, etc.) must be taken in order to acquire C1s data of organic monolayers without significant radiation damage.

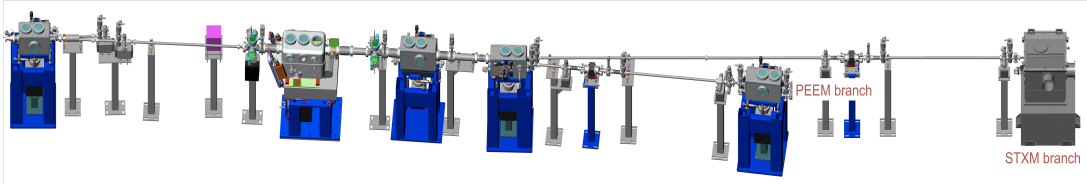

Figure 1.18 - SM beamline at the CLS depicting the PEEM and scanning transmission x-ray microscope (STXM) end-stations. (Figure adapted from C. Karunakaran, 2007)

1.6.2 Variable Line-Spacing Plane-Grating Monochromator (VLS-PGM) Beamline

The VLS PGM beamline is also located at the CLS[23,38]. It is a vacuum ultraviolet (VUV) to soft x-ray beamline capable of producing photons with energies from 5.5 eV to 250 eV. This makes it an ideal source for UPS studies. The beamline consists of a chicaned planar undulator, a plane grating monochromator, and the CaPeRS PEEM attached as an endstation (at the time of these experiments). The VLS PGM beamline with attached CaPeRS spectromicroscope (figure 1.19) were responsible for the majority of high-quality UPS and SEEM data in this thesis.

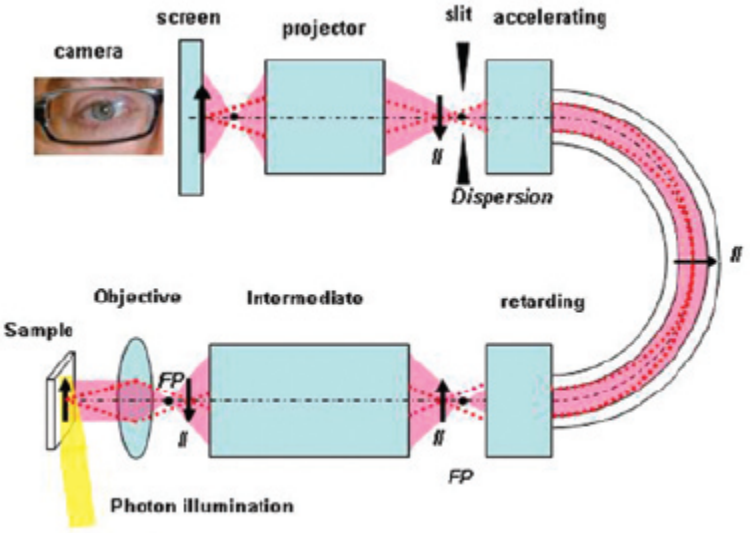

Figure 1.19 - Canadian Photoelectron Research Spectromicroscope (CaPeRS) energy-filtered PEEM microscope. Arrows indicate the images of the surface, dots the images of the back focal plane. (Figure adapted from S.G. Urquhart, 2008)

1.6.3 PEEM-2 Beamline 7.3.1.1

Beamline 7.3.1.1 is located at the ALS[25,39]. It houses the PEEM-2 endstation, which is capable of a spatial resolution as low as 50 nm. It is a bending magnet beamline, capable of producing elliptical, left circular, and right circular polarized light. The linear polarization is near 80% polarized, set by the adjustment of the x-ray slits at the front end of the beamline. As the beamline uses a bending magnet source, a 100 nm thick titanium filter was used for all C 1s experiments to filter out higher-order light. As the PEEM-2 microscope optics is unfiltered (no electron kinetic energy distribution), it similar to that depicted in figure 1.9. Most high-quality C 1s and F 1s NEXAFS data discussed in this thesis were acquired using the PEEM-2 spectromicroscope.

1.7 LB Systems

1.7.1 2AA1PA monolayer

The phase-separated monolayer system 2AA1PA, a 2:1 mole ratio mixture of AA and PA in 9:1 hexane:tetrahydrofuran(THF), was previously characterized by Qaqish and Paige using atomic force microscopy (AFM)[15]. In their studies, Qaqish and Paige used atomic force microscope height, friction, and selective dissolution experiments, to determine that hexagonal domains in the 2AA1PA system were in fact AA, and the continuous region surrounding these domains was the PA[15]. The dissolution experiments carried out by Qaqish and Paige identified the lipophobic domain by washing the sample with a non-polar solvent (hexadecane)[15]. This caused the removal of the arachidic acid domains, leading to a phase inversion in AFM images[15]. This data led to the assignment of hexagonal domains as AA and the continuous region surrounding these as PA. Although the system has been physically characterized by AFM height measurements, x-ray spectromicroscopy experiments provided complimentary chemical characterization of the phase identities[11].

This system was used for contrast mechanism elucidation, to better understand the effect of the CaPeRS PEEM energy-filter on organic monolayer samples. The

consistent formation of large hexagonal domains (<20 μm) surrounded by a continuous domain made 2AA1PA an ideal candidate for these experiments.

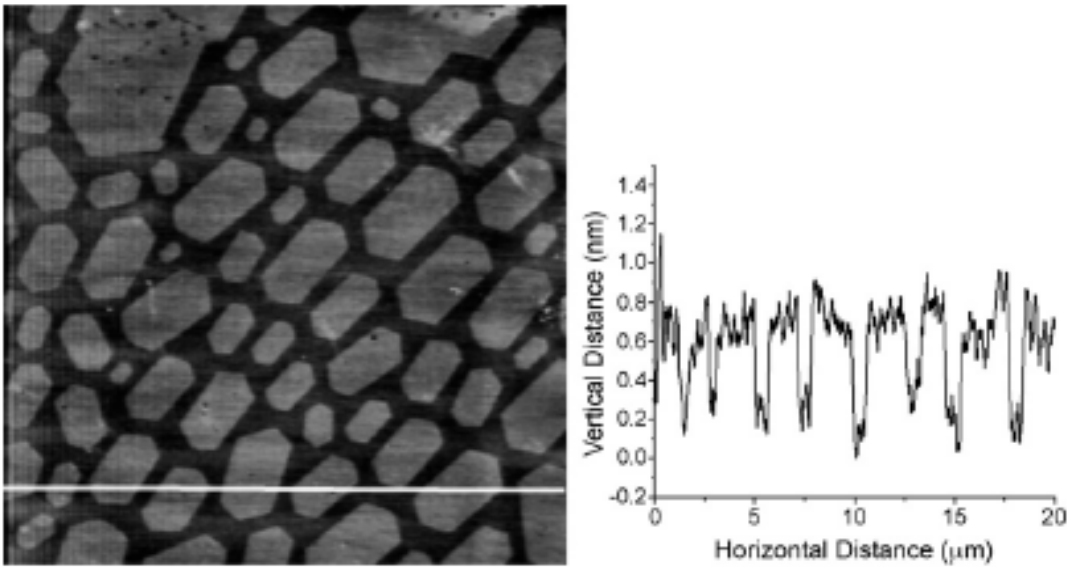

Figure 1.20 - AFM height mode image (20 μm x 20 μm, contact mode in air) and cross-sectional analysis of 2AA:1PA LB film deposited on silicon.

Initial AFM height measurements for these domains, using the scratch test method, adhesion force microscopy, and techniques in which one compound is selectively dissolved and washed from the sample[15,19], have determined the height of the hexagonal domains to be 22 Å, while the height of the continuous phase was determined to be 16 Å. This 6 Å difference in height between the two domains was measured with both mica and silicon substrates, confirming that the scratch test does not give erroneous height information by scratching into the substrate. Both molecules were measured to be shorter in length that those calculated using a theoretical method (discussed below); a difference of 3 Å in AA, and 2 Å in PA. Although very small and invisible at the scale shown in Figure 1.20, there are small domains of the same height as the discontinuous domains, mixed into the continuous phase. Previous quantitative studies of this by Qaqish and Paige have determined the composition of the continuous phase to actually be ~87% PA and ~13% AA.

The primary purpose of the height measurements was to identify the orientation of the molecules. LD-NEXAFS experiments would be more effective, as it provides direct information on orientation within the different domains of the system.

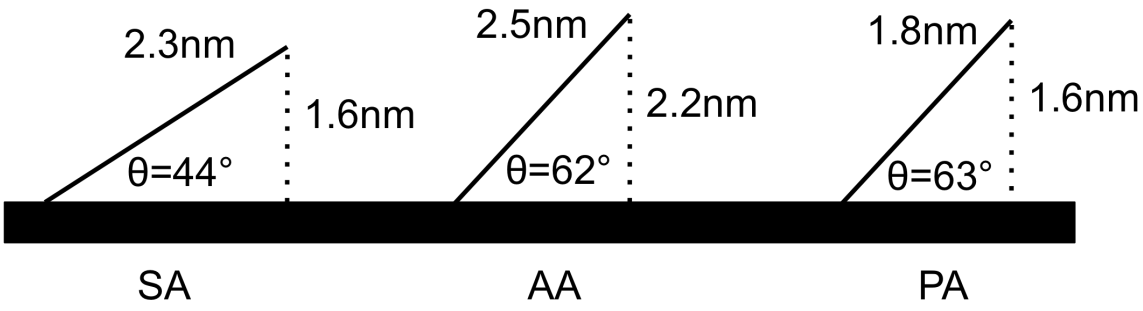

Figure 1.21 - Molecular angles based on AFM scratch test measurements of actual molecule height, and Hartree-Fock 6-31G* calculations of AA, PA, and stearic acid (SA) molecule lengths in a vacuum. These are approximate and only consider the molecules as straight rods.

Hartree-Fock 6-31G* calculations, using Spartan '06 for molecules in a vacuum, were used to calculate the theoretical lengths of the AA and PA free molecules. It is important to note that the required accuracy was in the Angstrom scale, and therefore an approximate calculation was adequate. Hartree-Fock calculations, using the 6-31G* basis set were expedient and take into account the helical conformation of long-chain perfluorocarbons. The calculations predict the molecule lengths to be 25 Å for AA and 18 Å for PA, corresponding to a ~7Å difference from the 22 Å of the AA, and 16 Å of the PA. The difference between theoretical predictions and experimentally determined height measurements could be explained by packing arrangement, conformation, or even tip-sample interaction.

Spatially resolved NEXAFS aquired using an X-PEEM microscope was used in order to determine the phase composition. Figure 1.22 demonstrates the power of a full-field imaging spectromicroscope for organic thin-film systems. The image is very similar in scale and contrast to the AFM image when illuminated with photons

of an appropriate absorption energy; 288.1 eV is the absorption energy of the $C1s \rightarrow \sigma^*_{C\text{-}H}$ transition[11].

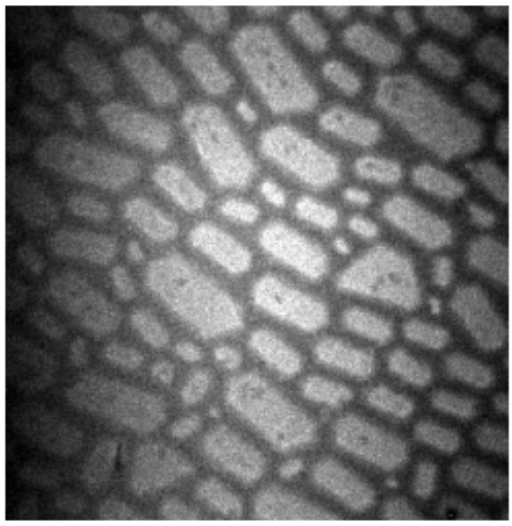

Figure 1.22 - X-PEEM image of the 2AA:1PA LB film, recorded with photon energy of 288.1 eV. The image is 29.3 μm wide.

The contrast in figure 1.22 is a convolution of the photoabsorption cross-section, workfunction and topography on the sample surface. The photoabsorption cross-section is based on the x-ray absorption cross-section. However, absorption leads to more secondary electron emissions. The contrast is sensitive to film thickness as a function of sampling depth. Although the contrast of the discontinuous domains is always greater, the relative difference in contrast varies with NEXAFS transition intensity.

1.7.2 2SA1PA monolayer

The 2SA1PA system, comprising of a 2:1 ratio of stearic acid (SA – $C_{17}H_{35}COOH$) to PA, phase-separates into linear domains with an average width of 300 nm. During the course of this thesis work, the film was physically characterized by AFM[19], through the use of selective dissolution. It was determined that there is a significant amount of SA in the PA domains. As with the 2AA1PA film, a more thorough chemical characterization using NEXAFS spectroscopy would compliment

this data. Initial AFM results determined the height of the SA domain to be 16 Å, while Hartree-Fock 6-31G* calculations determine the SA molecule to be 23 Å long. This discrepancy means that, should the molecules be perfectly straight, they are laying at an angle of 44°. Techniques such as XLDM-PEEM would be useful in direct measurements of molecular orientation.

1.8 Summary

Using well-understood PEEM-based NEXAFS spectroscopy, the properties of both semi-perfluorinated phase-separated LB monolayers, as well as those of the microscopes used for their characterization, are investigated. The small size of domains in the 2SA1PA sample, and therefore the absence of spatially resolved spectromicroscopic data, make 2SA1PA a good model sample to characterize using well-established PEEM-based NEXAFS methods. The spectrum-subtraction method was used to determine the spectrum of individual phases which are un-resolvable spatially using the PEEM-2 microscope at the ALS.

The previously well-characterized 2AA1PA sample was used to study contrast mechanisms in the energy-filtered CaPeRS microscope. Using UPS and SEEM techniques, these contrast mechanisms were better understood. The valence character of the 2AA1PA system was determined using UPS, while SEEM was used to explore contrast from secondary processes. Finally, an initial study into the molecular orientation of phases in the 2AA1PA and 2SA1PA films was conducted to determine the polarization dependence of the AA, PA, and SA domains.

Chapter 2 Application of Established PEEM-Based Measurement Techniques for Characterization of New Samples

2.1 Introduction

X-PEEM methods have gained popularity in the surface science community for the spatially resolved determination of surface structure and composition in the nm to μm scale[5,9,10,11,13,26,40]. Established complimentary surface spectroscopy techniques such as NEXAFS and angle-resolved NEXAFS (i.e. XLDM) enable the determination of both surface composition and molecular orientation[17,18,32,41,42,43,44].

One of the main goals of this project was to use these well-understood PEEM methods for the complimentary characterization of a poorly understood phase-separated LB monolayer, and XLDM to determine the molecular orientation in the separate phases. The film, 2SA1PA, originally physically characterized by Qaqish and Paige, was found to phase-separate into linear domains with significant domain mixing[19]. These domains were measured to be only 0.3 μm wide, but extended tens of microns in length. In this chapter, the determination of phase identity using NEXAFS and dissolution methods will be described, as well as what was done to determine the molecular orientation of the two phases.

2.2 Film Preparation

2.2.1 Langmuir-Blodgett Trough Setup

The Langmuir-Blodgett trough consists primarily of the trough, barriers, dipper, Wilhelmy plate and temperature controller. The trough and barriers are made of PTFE so as to be chemically inert and easy to clean. The trough and barriers need to be cleaned thoroughly before each use. Each piece was washed using warm water, distilled water, and finally isopropyl alcohol to ensure a dry and clean surface. Millipore water (18.2 MΩ/cm) was used as the subphase.

A vertically moving dipper, also made of PTFE, was positioned above the well (figure 1.1) to enable film deposition. The Wilhelmy plate was immersed in the

subphase close to the substrate, so that surface pressure readings were as close as possible to those encountered by the substrate. The Wilhelmy plate will be discussed more thoroughly in section 2.2.2 below.

The temperature of the water subphase was controlled by circulation of water through the external jacket of the trough. The water temperature was controlled by a water basin thermo-controller, and was measured *in-situ* by a thermocouple. All parameters and measurements were controlled through the KSV WINLB software package, including surface pressure, barrier speed and position, and dipper speed and position.

2.2.2 Surface Pressure-Area Measurements

The surface pressure is measured by means of a Wilhelmy plate, usually made of platinum, or clean filter paper. The Wilhelmy method is effective as long as the plate or plate-substitute has a roughened surface and does not contaminate the system. Platinum was used for these experiments, as it can be reproducibly cleaned using chloroform and a propane flame.

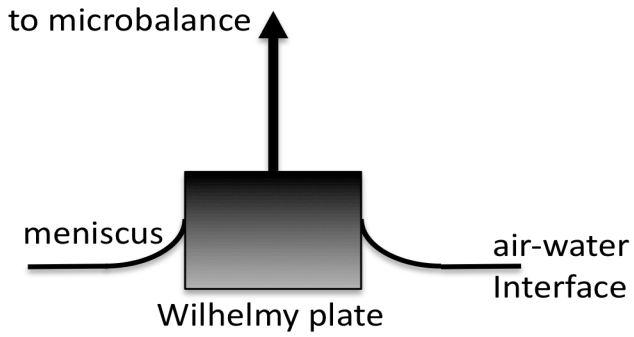

Figure 2.1 - Diagram representation of Wilhelmy plate arrangement at the air-water interface.

As shown in figure 2.1, water subphase forms a meniscus with the suspended Wilhelmy plate. The mechanism by which this method measures surface pressure is by monitoring small changes to the effective weight of the plate. The weight is determined by the net force acting on the plate, which includes the gravitational and

surface tension forces pulling the plate towards the subphase, and the buoyancy force resisting these. As mentioned above, the addition of a surfactant solution to the surface of the subphase reduces the surface tension of the system, therefore reducing the pull of the subphase on the plate. The plate then appears lighter to the scale as surface pressure increases.

2.2.3 Solutions

The solutions used in these experiments were prepared from materials purchased from chemical distributors. Arachidic acid (99%) and perfluorotetradecanoic acid (97%) were purchased from the Sigma-Aldrich Corporation, and stearic acid (99%) was purchased from BDH Chemicals Ltd, and used without any further purification. The dissolution solvents were hexanes (HPLC grade) from EMD Chemicals Inc., and tetrahydrofuran (THF) from Merck EM Science.

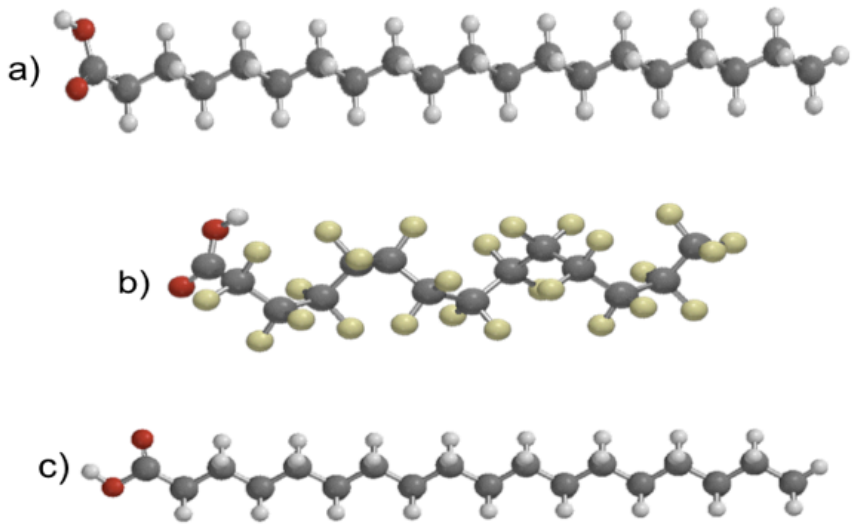

Figure 2.2 - Spartan '06 Ball and Stick model representations of a) arachidic acid, b) perfluorotetradecanoic acid, and c) stearic acid.

The 2AA1PA solution was prepared by the dissolution of 69.7 mg arachidic acid (2.23×10^{-4} moles) and 89.7 mg perfluorotetradecanoic acid (1.26×10^{-4} moles) in a 25 mL 9:1 solution of THF:hexanes. The solvents were chosen because of their

volatility, and their ability to dissolve the surfactants. A 30 μL aliquot of this solution was then spread on the air-water interface using a micro-syringe to disperse very small droplets (~3 μL/drop). The solution was settled for ten minutes to ensure adequate dispersion of the solute, and time for the solvent to evaporate. This method was used as it was shown by Qaqish and Paige to yield reproducible phase-separated films[15].

To obtain a compressed monolayer for deposition, the barriers slowly compressed the film at a rate of 10 mm/min, until the desired surface pressure was obtained. The rate of compression was slow, as more rapid movements cause deformation of the subphase, and therefore extra pressure or stress points for the film to collapse. Once the desired compression was achieved, 10 minutes was allowed for the film to stabilize. The software monitors the surface pressure, making small variations to barrier position to ensure a constant surface pressure.

The solutions remained stable for months, and yielded reasonably reproducible samples as long as their storage flasks were covered to prevent solvent evaporation. It was empirically determined that any shaking of the solution yielded smaller domains than usual, so motion of the flask was kept to a minimum.

Polished and cleaned phosphorus-doped silicon (Silicon Inc.) was used as a deposition substrate, as it is relatively smooth, low-cost, abundant, and easy to clean, as well as being a semiconductor and hydrophilic. The reason that hydrophilicity is important is that, as shown in figure 1.1, amphiphilic molecules align on the air-water interface. If the desired arrangement is that the hydrophilic head groups physisorb strongly to the substrate, a hydrophilic substrate is required (e.g. silicon, mica). If the desired arrangement is the hydrophobic tail groups on the substrate, a more hydrophobic substrate is necessary (e.g. gold). The semi-conductivity of silicon is important so that the samples do not build up a positive charge in the PEEM, as electrons lost during photo-ionization processes can be replenished through the conductive or semi-conductive substrate.

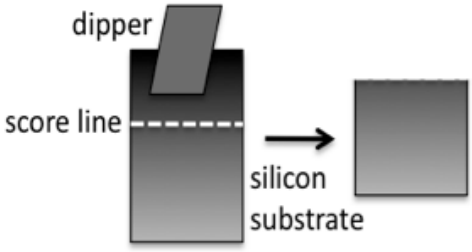

Figure 2.3 - Substrate dipper with score line demonstrating that the top portion of the silicon is removed to give a completely covered silicon substrate.

2.2.4 Substrate Preparation

When choosing the solid substrates upon which the films were to be deposited, consideration was required as to the conditions the samples would be subjected. While previous studies of the 2AA1PA and 2SA1PA films were conducted on freshly cleaved mica[15,19], an atomically flat and hydrophilic surface that is well suited for AFM studies, it is an insulator and therefore could not be used for electron spectroscopy. Insulators build a significant charge as electrons are photo-ejected from the substrate, and with no conducting source of electrons it becomes increasingly difficult for electrons to leave the sample as the surface charge increases. A conductor or semiconductor is ideal, as it can replenish the charge lost to photo-ejection. Silicon, due to its relative flatness, cleanliness, and semi-conductivity, was chosen as the substrate for these experiments.

The silicon was cut from large silicon wafers into ~8 mm x 8 mm squares using a diamond knife. The sample size was based on the size of the X-PEEM sample holders. The size constraints, along with the area used by the dipper (discussed below in section 2.2.5), left little of the sample area for actual measurement. The silicon was cut into longer rectangular pieces, which were then scored on the back face, so that there was one area that was 8 mm x 8 mm (figure 2.3). The remaining area was used as a clipping area for the dipper, and was later broken off in a very careful manner so that only a completely covered perfectly sized square remained for experimentation. This effectively increased the sampling area, allowing for fewer sample changes and therefore saving valuable beamtime. The

edges of the sample holder where also avoided as electrons from the titanium cap and electric field gradients affect PEEM contrast and focus.

Dust was removed using a compressed air duster (1,1-difluoroethane 75-37-6, Grand & Toy). Cleaning was by sequential sonication in trichloroethylene, acetone, and ethanol, for twenty minutes each. Trichloroethylene was used because it is a known degreaser and would remove hydrophobic debris on the substrates. Acetone was then used to remove any remaining trichloroethylene and organic debris. Finally ethanol was used to remove any of the remaining organic debris and acetone. The substrates were dried under nitrogen gas, and then examined under an optical microscope. The final step was illumination under an Hg-arc lamp, as it creates ozone, which then destroys any remaining organic components, creating CO_2 gas. Once cleaned, the samples were ready to be used for LB depositions.

Mica was used for most AFM measurements that were not to be studied by PEEM. The atomically smooth and clean substrate allowed more accurate height measurements with less noise, however they were not used for PEEM measurements, as mica is an insulator.

2.2.5 Mounting and Dipping

As described in section 2.2.1, the vertical dipper is constructed of PTFE, to reduce the chances of chemical interaction or contamination from dipper to sample, or worse yet, dipper to air-water interface. When the subphase and monolayer are ready for deposition, the sample (attached to the dipper) is pulled through the air-water interface, depositing the polar head groups onto the hydrophilic silicon surface. If more layers are required, this process can be repeated.

When fresh samples are deposited, they are stored in clean Petri dishes and wrapped in Parafilm® to avoid surface contamination. Samples were prepared as close to beamtime as possible. Because of the number of samples needed, and the ~2 hours that each sample requires from deposition to AFM characterization, a dipper capable of dipping multiple substrates was developed. The multi-dipper, capable of preparing up to 3 samples at a time, was used successfully as long as adequate spacing was allowed between substrates, and the values given to the WINLB software

accounted for the change in the total substrate surface area. The dipper (figure 2.4) consisted of a butterfly clip with its edges softened by duct tape, and a bent metal wire to hold it perpendicular to the subphase surface.

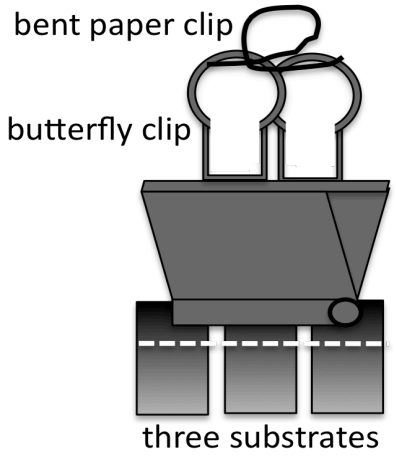

Figure 2.4 - Diagram of multi-dipper setup, including three substrates for simultaneous dipping.

The substrate was mounted on a PTFE clamp, enabling the vertical movement of the substrate into, and out of, the air-water interface. The dipping procedure withdrew at a rate of 4mm/min. The films were deposited at a constant surface pressure of 20 mN/m for the 2AA1PA film and 10 mN/m for the 2SA1PA film. Although it has been determined that dipping rate has an effect on domain size and orientation[19], values were chosen for these experiments on the sole criteria that they create monolayers with reproducible domain shape and size.

2.3 Atomic Force Microscopy (AFM) Experiments

2.3.1 Atomic Force Microscopy Setup

AFM height measurements were conducted in contact mode, on a Dimension Hybrid Nanoscope system (Veeco Metrology Group). The entire setup was isolated from noise by mounting it in an acoustic-vibration isolation system. The AFM cantilever probes were also Veeco brand; their tips consisting of Si_3N_4 with a 0.5 N/m cantilever spring constant.

Samples were first mounted on a glass slide with double sided tape. All samples were oriented in the microscope such that the vertical axis in images was the same as the sample withdrawal direction. Sample tilt was reduced as much as possible. The glass slide was then placed on the sample stage of the AFM and held in place by a slight vacuum pressure. The static position of the sample acts to reduce noise.

2.3.2 Contact Mode Imaging

In contact mode, the cantilever remains in contact with the surface of the sample at all times during the measurement. As the tip passes over the surface topography, changes in cantilever deflection are read by detection of positional changes to a laser being reflected off the cantilever. The technique provides high spatial and vertical resolution topography maps of the sample surface. The height of molecules relative to the substrate can be measured using a scratching technique – discussed previously in section 1.7.1. Control experiments indicated that the imaging process did not damage the sample surface. Some experiments, however, were designed to remove the sample film by applying a deflection set-point voltage of 9 V, as opposed to the 0 V used for regular height imaging in contact mode. This results in a large tip-sample interaction force which can remove the monolayer from the area being scanned. These conditions were used for scratch tests, so as to determine the thickness of the monolayer film above the silicon substrate.

2.3.3 AFM Cross-sectional Imaging

In order to determine the height differences between each domain, cross-sectional analysis was done. In this analysis, the height differences across a 2D slice of an AFM image is plotted. This type of analysis is valuable because it enables not only the determination of domain or feature height, but also a very accurate measurement of distance between features. Figure 1.20 in section 1.7.1 shows the value of this technique, as it is used, along with a scratching technique, to determine the differences in height between two domains, and between the substrate and the two domains.

2.4 PEEM

2.4.1 Sample compatibility

Samples measured in PEEM microscopes must meet certain conditions. As field emission from samples can lead to distorted images and spectra, and PEEM is very surface sensitive (<5 nm)[45,46], samples need to be clean, and flat. Sample flatness is generally achieved by polishing for metallic samples, or by preparing samples such as self-assembled monolayer, LB monolayer, or spin cast organic systems on planar substrates.

Samples also need to be conductive to prevent charging. The sample surface itself need not be conductive (non-conductive thin film), but as long as it is thin and is deposited on a conducting surface (Si, metals, etc.) the sample can be used.

Finally, samples must be solid and must not vaporize in vacuum. As pressures in the PEEM main chamber area regularly as low as 10^{-7} to 10^{-9} torr, caution must be observed in sample selection so as not to degrade the vacuum or contaminate future samples.

2.4.2 Halo Effect in PEEM

A "halo" effect is present in both the PEEM-2 and CaPeRS spectromicroscopes. When spatially resolved experiments are carried out, such as those using NEXAFS spectromicroscopy, there is a significant signal contribution (~10%) from outside the immediate field of view – a spatial averaging of signal. This effect has been attributed to internal scattering of electrons inside the lens system, by apertures or defects. The problem has been reduced in the CaPeRS microscope since September 2008, using field of view limiting apertures to reduce the size of the beam and therefore electron scattering inside the PEEM column.

2.5 Dissolution Experiments

Problems with the acquisition of spectra using PEEM-NEXAFS spectromicroscopy occur because of the small width of the SA and PA domains within the 2SA1PA system. The CaPeRS X-PEEM on the SM beamline is capable of

a spatial resolution of 30 nm, which is ideal for imaging systems such as the 2AA1PA system, where the hexagonal domains were ~6 μm in size. When domains are on the nanometer scale, such as the ~0.3 μm wide 2SA1PA domains, it is possible but very difficult for the microscope to resolve such small domains, and emphasis was placed instead on spectroscopic measurements.

One method to determine the spectrum of the different 2SA1PA phases is to selectively dissolve each domain and acquire the spectra of the undissolved phases separately. Therefore, the averaged spectrum of each domain is adequately represented, and in the proper proportion. The problem with this approach is that it is difficult to selectively dissolve the PA phase. While the hydrophobic SA is removable by using a non-polar solvent such as hexane or hexadecane, the hydrophobic and lipophobic character of the PA provides a challenge in determining an appropriate solvent that does not remove the SA phase as well.

A theoretical approach for solvent determination was considered, but after much research it was determined that a systematic, empirical approach would be more practical.

2.5.1 Common Solvents for Phase Dissolution

The approach used in these experiments was to empirically test the ability of various solvents to remove SA, PA or both. The selected solvents were toluene, pentane, hexane, and n-hexadecane. LB films were incubated in solvent for 5 minutes, after which the solvent evaporated and the sample imaged in the AFM to determine if the domains had dissolved. The next tests were with the polar solvents THF, water, and ethanol. Finally, simultaneously hydrophobic and lipophobic molecules, such as the perfluoroalkane solvents perfluorononane and perfluorooctane were used to determine if dissolution of PA occurred.

2.5.2 Hexadecane/Hexane Washing Technique

Qaqish and Paige used n-hexadecane to dissolve and remove AA and SA using *in-situ,*monitoring dissolution with AFM measurements[15,19]. These were performed in contact mode using a wet-cell AFM mount. Hexadecane has a low

vapour pressure, and therefore the film could be imaged without the evaporation of the solvent and redeposition of the dissolved SA (figure 2.5).

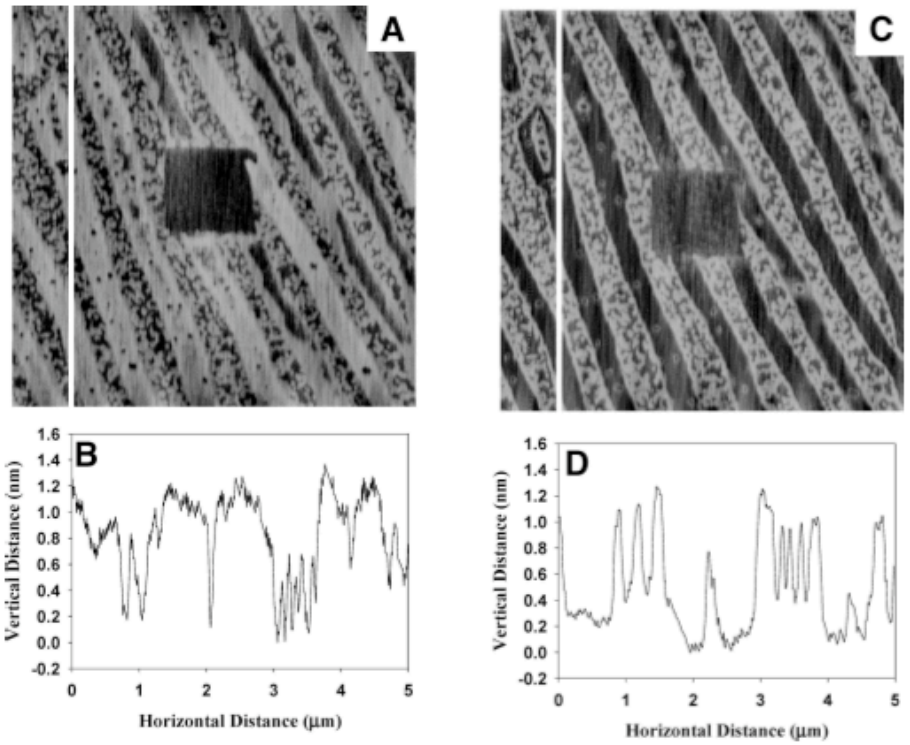

Figure 2.5 - AFM height mode images and their cross-sectional analysis are from Qaqish and Paige[19]. A) 2SA1PA in air with representative cross-section B), and C) 2SA1PA in hexadecane with representative cross-section D). All images are 5 μm x 5 μm. The centre feature is visible substrate where the film has been scrapped off in a 1 x 1 μm square. (Figure adapted from S.E. Qaqish, and M. Paige, 2007)

As samples used in PEEM are required to be vacuum compatible, and as the less volatile hexadecane would remain on the sample to contaminate the vacuum environment, hexane was used to remove the hexadecane. Clean hexadecane was gently deposited onto the sample surface using a micropipette. As hexadecane evaporates very slowly, it was left for 30 minutes to completely dissolve the SA phase, before being removed. To remove the hexadecane, the sample was propped at a 45° angle, and hexane was slowly and gently dropped over it using another clean micropipette. Caution was used so as not to strip the surfactant from the substrate by

applying the hexane too vigorously. This was repeated carefully for 10 minutes, after which the sample was stored in a desiccator over silica gel.

2.6 Dissolution Results and Discussion

2.6.1 Results of Common Solvents

Of the common non-polar solvents toluene, pentane, hexane, and n-hexadecane, all dissolved the SA domain quite readily, but after 5 minutes of washing the sample, the PA domains remained. The polar solvents THF, water, and ethanol were found to remove all surfactant from the substrate. The perfluoroalkane solvents perfluorooctane and perfluorononane, when used to wash the samples, removed nothing from the surface. Unlike the PA phase, they have no polar head group, and therefore have little interaction with the surface film.

Based on these results, it was determined that perhaps a longer or shorter-chain perfluoroalkane would remove the PA domains, but these solvents were cost prohibitive. Other methods were attempted (see subtraction method – section 2.8) instead of trying these solvents.

2.6.2 Washing Results

To ensure that washing the samples with hexadecane and hexane did not damage the sample, AFM was used to image the results. Figure 2.6 depicts the pre and post-wash images of the 2SA1PA film, demonstrating that the procedure does not destroy phase organization, but rather removes the SA from the film. AFM images were taken for each sample this procedure was used on, and no damage to the samples was observed.

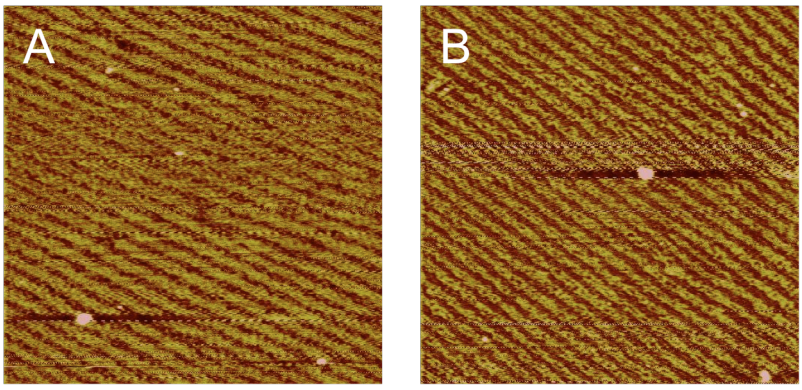

Figure 2.6 - AFM images of 2SA1PA system (5 μm x 5 μm, contact mode in air). Images are of A) 2SA1PA (pre-washing), and B) 2SA1PA (post-washing).

2.7 Discussion of Normalization Technique and Theory

In order to understand the C 1s spectra of the 2AA1PA and 2SA1PA systems, it is first important to understand that each spectrum is the product of the beamline function (I) and the sample's spectroscopic cross-section, as well as the procedure with which the workup is performed. If broken down, the measured signal is a composite of other functions, given by:

$$C1s = \sigma_C = \frac{(I)(\sigma_C)}{(I)(\sigma_{Au}) \Big/ (\sigma_{Au_{DB}})} \qquad (2.1)$$

The carbon signal is a product of the absorption cross-section of carbon (σ_C) and the beamline function (I). The beamline function is removed by division of the carbon signal from a clean gold substrate (I)(σ_{Au}). Finally, the cross-section of gold at the carbon-edge from the beamline, is divided by the cross-section of gold at the carbon-edge from the CXRO database[47].

Normalization of measurements are required to remove unwanted background signal. In carbon-edge measurements, carbon contamination on optics upstream to the microscope will absorb photons with carbon-edge energies, reducing the amount of flux in that energy range. Gold-coated silicon is used to obtain background measurements, as sample placement and experimental conditions can be replicated.

2.8 Viability of the Spectroscopic Subtraction Method

Because of the success of the dissolution experiments where SA is removed from the 2SA1PA monolayer, as well as the inability of PEEM to resolve the 2SA1PA linear phases, another method to measure the spectra of individual domains was devised. Theoretically, washing the 2SA1PA system with hexadecane to dissolve the SA domains, followed by hexane to remove the non-volatile hexadecane, should leave only the PA domains on the substrate. If the spectrum of a 2SA1PA monolayer is subtracted the spectrum of a washed sample (PA domains), the resultant spectrum should be that of the SA domains in the system.

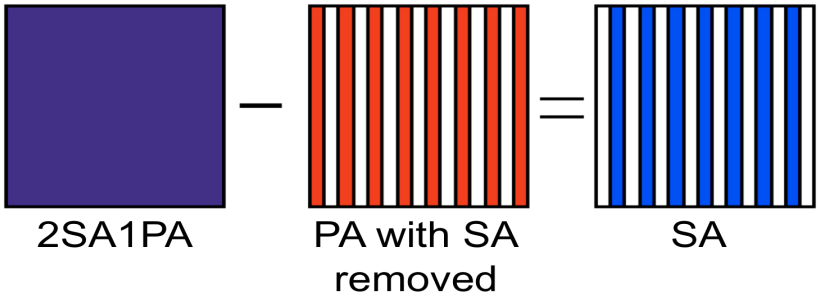

Figure 2.7 - Diagram demonstrating subtraction method, where spectrum of washed 2SA1PA sample (PA phase signal only) is subtracted from that of the entire 2SA1PA film, yielding the SA phase spectrum.

The viability of this method was first tested with the 2AA1PA sample, as the washing procedure is known to be effective in dissolving the AA phase of these samples. The resultant spectrum was previously compared with data from previous experiments[11]. 2AA1PA LB monolayers were deposited on silicon. Washing the samples with hexadecane, followed by hexane and AFM imaging, demonstrated the effectiveness of the washing technique, as well as determined the remaining material consisted solely of the PA domains.

2.9 Subtraction Method Viability Using 2AA1PA LB Films

2.9.1 2AA1PA Subtraction Method Experiments

The subtraction technique experiment was performed data acquired on the PEEM-2 ALS beamline 7.3.1.1. The flux, controlled by apertures upstream in the beamline, was reduced to a value of -0.5, an arbitrary index of which -0.5 is the minimum value, and 2.0 is the maximum value. As noted previously, a reduction in flux results in a change in polarization, as bending magnet sources polarization varies vertically, and different entrance slits will vary the x-ray polarization. The exact percent the beam was polarized linearly is not known, although it is below 85% in the horizontal plane.

C 1s spectra were taken of a pristine region of the film from 280 eV - 300 eV. In order to reduce the effects of radiation damage, the energy scale was scanned coarsely in 1 eV steps from 280 eV – 285 eV, in 0.5 eV steps from 285 eV – 293 eV so that fine-structure in that region was represented, and in 1 eV steps from 293 eV – 300 eV. Although each scan had a dwell time of 1 second to improve counting statistics, the total scan duration was less than 3 minutes. To test the reproducibility of the spectra, nine spectra were taken on different fresh regions of the sample.

Also of interest during these experiments was the effect that intermolecular interactions have on the spectra of PA molecules. To explore this effect, the spectra of PA were gathered from three different sources. Figure 2.8 depicts the spectra of PA extracted using the aXis2000 software package (2AA1PA Continuous Phase), PA from a pure film (PA), and PA remaining after the washing of a 2AA1PA sample by hexadecane and hexane (PA from AA-subtracted 2AA1PA). The software package aXis2000 was used to develop masks of regions of interest, so that only the spectra from selected areas is displayed. These techniques were then used to select the spectra of the PA-rich continuous phase. The spectrum of the pure PA monolayer was obtained by averaging the spectra of PA over a 20 μm area. Finally, the spectrum of PA surrounded by empty silicon substrate was obtained by the washing of a 2AA1PA sample with hexadecane and hexane, thus removing the AA and leaving the continuous PA domain with large areas of uncovered silicon substrate.

As the environment surrounding the PA domains is removed with washing, F 1s NEXAFS spectra were obtained from the 2AA1PA-washed system, as complimentary support that the perfluorinated PA molecules remain on the sample surface (see figure 2.8 below). The Ti filter was retracted, as it filters out radiation with energies above the Ti 2p edge. A F 1s NEXAFS scan was run from 683 eV – 686 eV with 1 eV steps, and 686 eV – 708 eV with 0.5 eV steps.

2.9.2 2AA1PA Subtraction Method Results and Discussion

The subtraction method can be a viable alternative if the domain of interest cannot be spatially resolved. The 2AA1PA signal (black) is comprised of the sum of the PA spectrum (red), obtained by removal of the AA using the hexadecane/hexane washing technique, and the AA signal (blue) from a pure film. Intensity is measured in arbitrary units, as this method is not quantitative, and intensity matching is required in order to process and manipulate the data. The peak at 292.8 eV is attributed to the C 1s$\rightarrow\sigma^*_{C\text{-}F}$ transition in PA[11]. In figure 2.8, it is evident that this feature is much more pronounced in the 2AA1PA and 2AA1PA-AA washed systems. This is as expected in the perfluorinated systems, adding confidence that PA is remaining on the substrate surface. The other large peak, at 288 eV-289 eV is the C 1s$\rightarrow\sigma^*_{C\text{-}H}$ transition typical of AA (and SA)[11]. The PA peak (red) at 289 eV is low, relative to those of the 2AA1PA and AA systems (black and blue respectively), which has previously been seen in the literature[11] as the C 1s$\rightarrow\sigma^*_{C\text{-}H}$ transition. In AA, the peak at 292.8 eV (blue) is markedly reduced in comparison to the 2AA1PA (black) and PA (red) spectra. This reduction also lends confidence that the AA spectrum contains little signal contribution from PA molecules. Figure 2.8 shows AA spectra that were obtained from the subtraction of the 2AA1PA and 2AA1PA-washed spectra, confirming the viability of the subtraction method to characterize domain composition when domains cannot be spatially resolved.

The data in figure 2.8 indicates that the subtraction method can elucidate the spectrum of one phase by the subtraction of the system spectrum by that of the other phase.

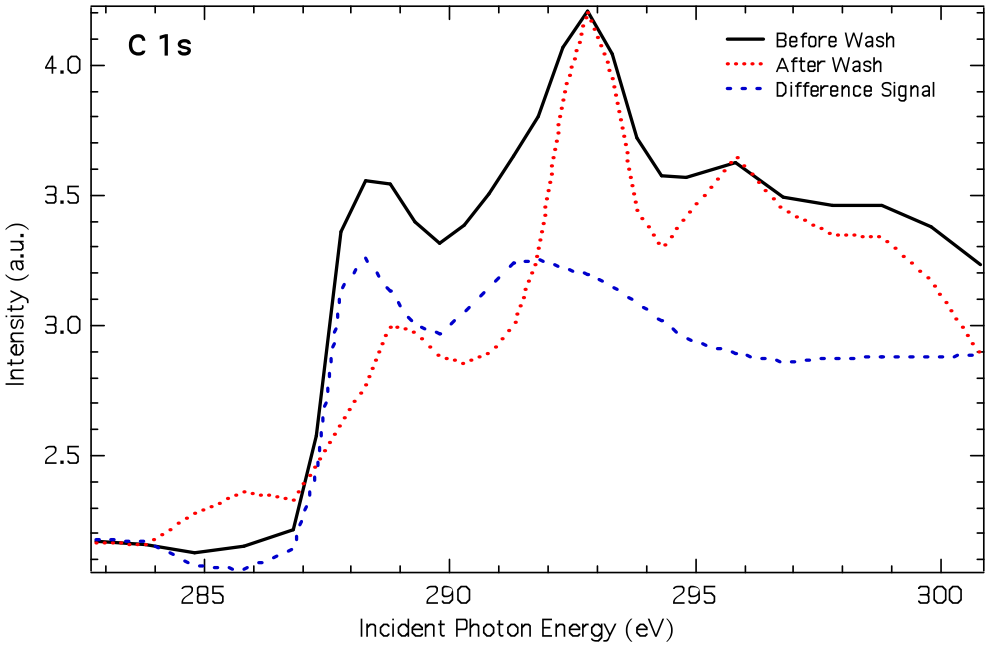

Figure 2.8 - C 1s NEXAFS spectra of 2AA1PA (black), 2AA1PA washed with hexadecane and hexane leaving only a PA signal (red), and the resultant AA signal produced by the difference (blue). Spectra recalibrated to C1s → σ*C-F = 292.8eV and rescaled[18].

Figure 2.9 shows the F 1s spectrum of a 2AA1PA-washed sample. As was suggested in figure 2.8 by the strong presence of a C 1s→$\sigma^*_{C\text{-}F}$ transition at 292.8 eV, the F 1s spectra shows a peak in the 2AA1PA-washed sample. As assignments for the peaks at 690 eV and 694 eV have yet to be determined, the F 1s absorption cross-section was included to demonstrate qualitatively that there is significant feature signal contribution. The absorption cross-section data obtained from the Center for X-Ray Optics (CXRO) database[47].

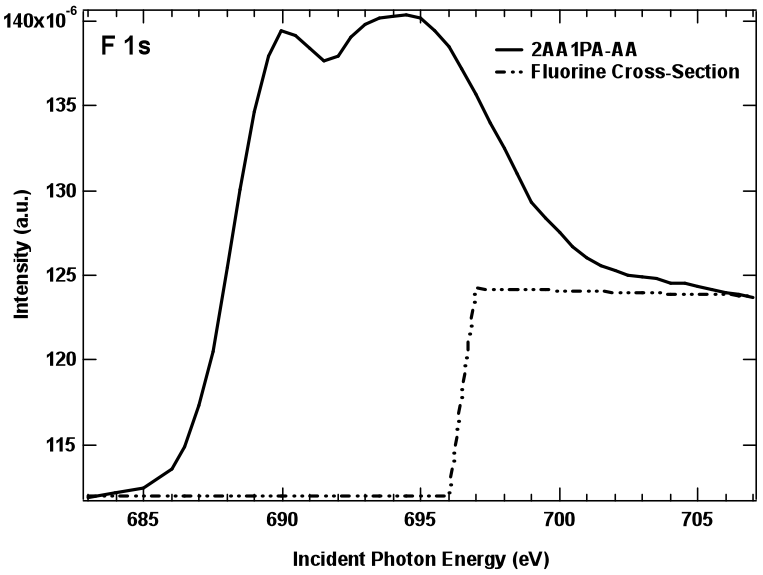

Figure 2.9 - F 1s NEXAFS spectrum in 2AA1PA LB film including F 1s cross-section calculated using CXRO parameters[47].

The PA spectra from three different PA systems were compared in order to determine if there were any differences in the C 1s NEXAFS spectra with variations to the local environment surrounding the PA molecules in each spectrum (see figure 2.10 below). The C 1s NEXAFS spectrum of PA, masked from the 2AA1PA system and therefore surrounded by AA molecules, is represented by the solid black spectrum in figure 2.10. PA from 2AA1PA washed samples, where AA has been removed by selective dissolution, is surrounded by uncovered substrate due to the washing technique (blue dotted line in figure 2.10). Finally, the spectrum of PA from a pure PA film, and therefore only surrounded by other PA molecules is represented in figure 2.10 by red dashes. C1s PA NEXAFS spectra were compared from the masked continuous phase of a 2AA1PA phase-separated film surrounded in part by AA molecules, a pure and completely homogenous PA film, and the PA from a washed 2AA1PA sample, where PA is surrounded by areas of uncovered substrate.

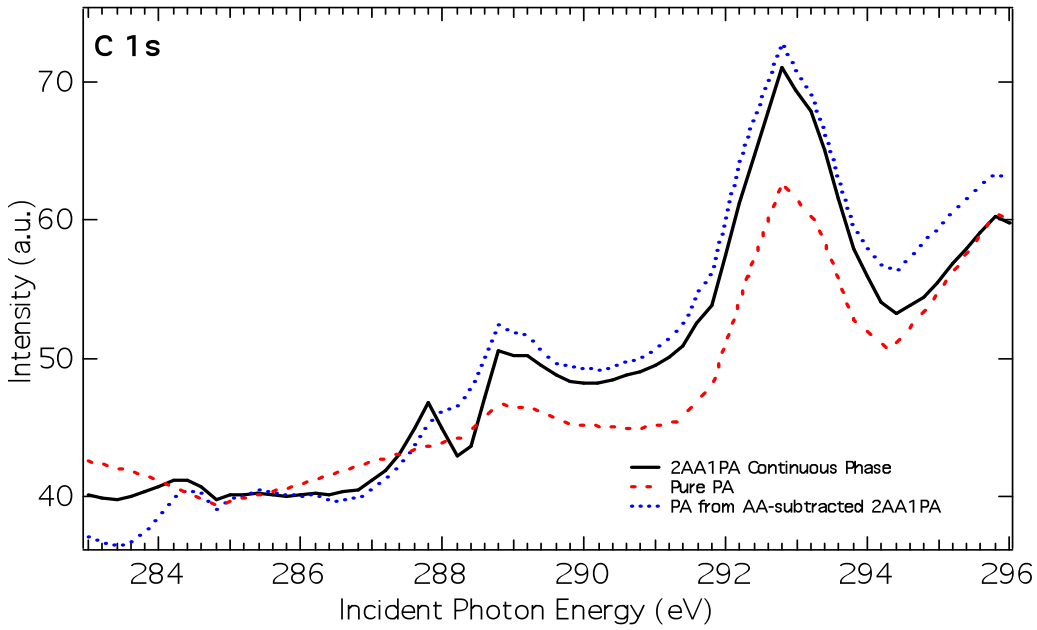

Figure 2.10 - C 1s NEXAFS spectra of 2AA1PA continuous phase (black), pure PA (red), and the PA signal from using the subtraction method (blue). Spectra recalibrated to C1s → σ*C-F = 292.8 eV[18].

Peak intensities in the PA spectra demonstrate that the change in PA environment surrounding affects the PA domains. The features at 287.8 eV, 288.8 eV, and 292.8 eV in figure 2.10 seem to be sharper and more pronounced in the 2AA1PA continuous phase. The flat pre-edge at 286 eV for the pure PA sample is evidence that there is less relative radiation damage in the pure film than in the 2AA1PA continuous phase spectrum or the 2AA1PA-washed subtraction spectrum. Although there are differences between the spectra, they are small, and present themselves primarily as radiation damage. The ability to use the subtraction method to obtain identifiable spectra is a novel approach for phase-separated systems characterization, where spatial resolution of phases is difficult.

2.10 2SA1PA Composition Characterization

2.10.1 Experimental Determination of 2SA1PA C 1s Composition by NEXAFS

In order to fully understand the contributions of SA to the C1s NEXAFS of the 2SA1PA system, the spectrum of pure SA was determined. An SA monolayer

was measured on the PEEM-2 using similar parameters as the 2AA1PA C 1s system discussed in section 2.3.1. The titanium filter was inserted, and the flux set to -0.5. The scan was run with 1 eV steps from 280 eV to 285 eV, 0.5 eV steps from 285 eV to 293 eV, and 1 eV steps from 293 eV to 230 eV, with a dwell time of 1 second for each step. Left circular polarized (LCP) radiation was used as it can alternately be considered as non-linearly polarized light, and therefore should not excite any features preferentially.

2.10.2 Results and Discussion of Pure SA C1s NEXAFS Contribution

The spectrum shown below (figure 2.11) shows a large C 1s→σ^*_{C-H} peak at 287 eV. Due to the short dwell times required to reduce sample radiation damage, the signal-to-noise ratio is low. The SA spectrum in figure 2.11 has been 3-point smoothed to remove noise from the original spectrum. The weaker signal (higher relative noise) compared to other monolayers under the same scan conditions[11] suggests that the SA molecules may be laying at a severely acute angle to the substrate surface. This would explain the low absorption signal, as the sampling depth is reduced compared to AA and PA.

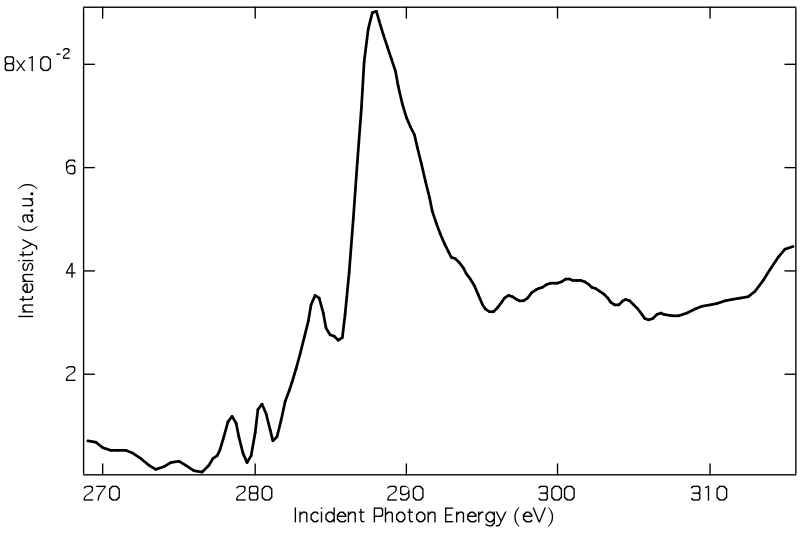

Figure 2.11 - C 1s NEXAFS spectrum of SA film. Spectrum was 3-point smoothed. Spectra recalibrated to C1s → σ^*_{C-H} = 288 eV[18].

The resulting pure SA film shows a very large C 1s→ σ^*_{C-H} peak at 288 eV. The spectrum features at 285 eV is due to radiation damage of the sample, as removal of a fluorine or hydrogen atom causes saturation (double bond formation) of the surfactant molecule, and the subsequent C 1s → $\pi^*_{C=C}$ bond is visible at 285 eV.

2.11 Molecular Orientation Experiments

X-ray linear dichroism microscopy (XLDM) experiments, performed using NEXAFS spectroscopy on an X-PEEM, require linearly polarized light. These can be performed with either the use of bending magnet linear polarized light (PEEM-2) which is only ~80% horizontally polarized, or an elliptically polarizing undulator (EPU) such as that found on the SM beamline (100% +0/-1%). As discussed in section 1.4.2, the relative intensity of near-edge features can reveal molecular orientation. As beamline 7.3.1.1 emits only horizontally linear polarized light, as well as right or left circularly polarized light (RCP and LCP respectively), LCP or RCP can be considered as non-linearly polarized radiation, and the experiment becomes one of linear vs. non-linear polarization.

Because of the relatively low signal of the SA films and AFM results, the SA molecules are likely lying at an angle, XLDM experiments were done on pure SA films, as well as pure PA and 2SA1PA. The experiments were again performed at the ALS, as ~80% linear polarization is enough to determine the feasibility of these studies. The incident photon angle will also hinder the experiments, because if the molecules are normal to the sample surface, an incident angle of 30° (PEEM-2) will show less polarization effect than a 16° incident angle (CaPeRS).

2.11.1 PA XLDM Experiments

Short scans were taken using the PEEM-2 microscope, with 0.5 s dwell times, and a relative flux increment of 0.0. 13 scans were taken sequentially so as to dynamically determine differences in acquired PA spectra. Scans were taken in the same manner as previous experiments, the difference being that each spectrum was acquired under both linear polarization, and non-linear (LCP) polarization. The

resultant spectra demonstrated that there were no real noticeable differences between damage from the linear and LCP radiation over a sub-20 minute exposure time period. The results are shown in figure 2.12.

2.11.2 PA XLDM Results and Discussion

Figure 2.12 demonstrates the linear and LCP polarization dependence of the pure PA system and explores the effect of polarization on the radiation damage. In the linearly polarized spectra, the C 1s $\rightarrow\sigma^*_{C\text{-}F}$ peak at 292.8 eV decreases by 61.5% over a 20 minute time period, while the decrease is 59.3% when non-polarized light is used. The small relative change in peak intensity at 296 eV (81.2% decrease vs. 83.5% decrease) and 299 eV (73.3% decrease vs. 73.1% decrease) mean that changes due to radiation damage are greater than those that would be observed due to polarization dependence. The weak angular dependence may be due to the <80% polarization of the linear photons inherent in a bending magnet beamline, even with slits to control radiation damage.

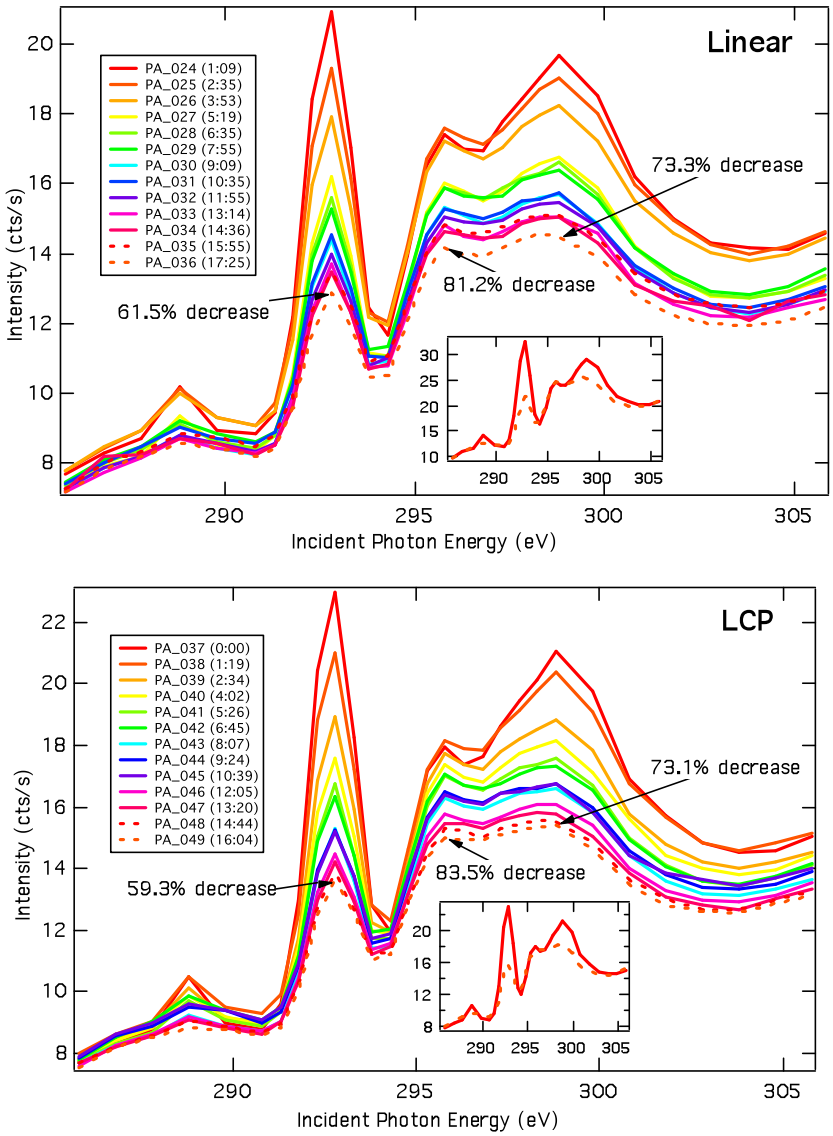

Figure 2.12 - Graph of C 1s NEXAFS for pure PA LB monolayer with radiation damage by linear and LCP photons. 0.5 s dwell, consecutive scans, new region for LCP experiment. Inset graphs show differences between first and last scans, scaled at pre and post edges. Spectra recalibrated to C1s → σ*C-F = 292.8 eV[18].

The helical structure of PA may be another factor playing a role in this lack of polarization dependence[18,27]. Linear dichroism experiments become less sensitive, as the induced transition dipole moments (TDM) of the C-F and C-C x-ray absorption transitions were not perpendicular to each other, and the signal was therefore a product of both the C-F and C-C transitions. Ziegler et al. were able to

determine the polarization dependence of oriented PTFE using linear dichroism experiments[18]. Unlike the Ziegler paper[18], the molecules present in the 2AA1PA LB monolayer system may be isotropic in nature. Isotropy averages the signal over many different vectors, resulting in spectra with little evident polarization-dependence. The AA and SA molecules are in a zig-zag conformation, meaning that the C-C backbone is perpendicular to the C-H bonds[17]. As depicted in figure 1.12, this perpendicular arrangement leads to polarization dependence with changes with linear polarization. Changes in polarization-dependent NEXAFS spectra are therefore more evident in the SA and AA spectra.

Finally, differences in LD- NEXAFS spectra may be difficult to elucidate if the molecular orientation is more isotropic in nature.

The difference in signal may possibly be due to mass loss in the radiated area. Each scan was divided by its initial ring current, so there should be no effect from ring current decay. As it has been shown to be quite a difficult experiment to determine the orientation of PA molecules under these conditions, experiments were continued with the SA sample, as beamtime was limited.

2.11.3 SA XLDM Experiments

LD experiments on SA were conducted using the same conditions as the previous C 1s NEXAFS scans. The titanium filter was inserted, with the flux turned down to -0.5. The scan was run from 280 eV to 285 eV with 1 eV steps, from 285 eV to 293 eV with 0.5 eV steps, and from 293 eV to 230 eV with 1 eV steps. The experiment parameters were similar to the PA XLDM experiments, although for these experiments the dwell time for each step was 1 s.

2.11.4 SA XLDM Results and Discussion

The spectra in figure 2.13 are the linear and LCP C 1s NEXAFS spectra of SA. The difference in the spectra is the reduction of the 288 eV peak with linear polarization. As previously stated, the low signal is most likely due to the thickness of the SA film. This reduction of peak intensity with linear polarization supports the theory that the molecular orientation is at an acute angle, and that the molecular

arrangement is somewhat random. The exact angle and the extent and order of the molecular arrangement are still unclear, and would take experiments on the CaPeRS X-PEEM for determination. The incident angle is not shallow enough, and the polarization not pure enough to determine more than that there is some polarization dependence in the SA samples, which was the purpose of these experiments.

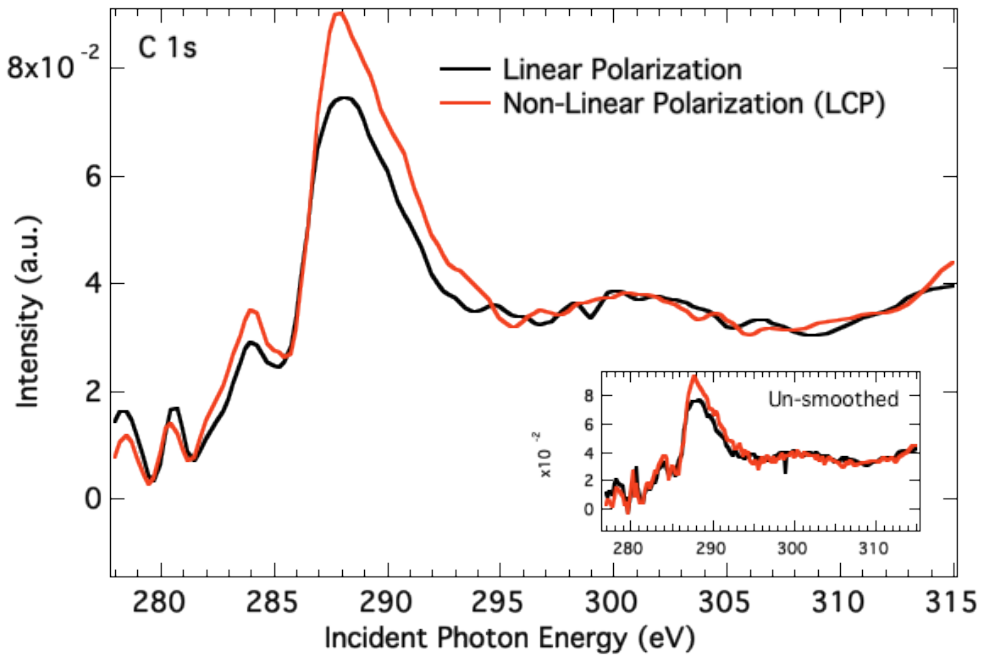

Figure 2.13 - C 1s NEXAFS spectra of SA on silicon, using linear and left-circular polarized x-rays. The embedded graph is the original normalized spectra. The larger graph spectra are the same data, with 3-point smoothing. Spectra recalibrated to C1s → $\sigma^*_{C\text{-}H}$ = 288 eV[18].

2.11.5 2SA1PA XLDM Experiments

As AFM height information suggests, the angle at which the molecules are oriented may depend on the organization of surrounding molecules. The 2SA1PA film is an example of this, as the SA C 1s NEXAFS data suggests that it is lying down; while AFM measurements suggest the PA molecules are aligned normal to the substrate[15]. The AFM measurements of the 2SA1PA film seem to support that all molecules are lying down.

The C1s NEXAFS of 2SA1PA was determined using the same experimental setup as section 2.4.3. (280 eV – 285 eV with 1 eV steps, 285 eV – 293 eV with 0.5 eV steps, 293 eV – 300 eV with 1 eV steps). The dwell was again 1 second, with the Ti filter in and flux set to -0.5.

2.12 Summary

The goal of the research highlighted in this chapter was to use established and well-understood PEEM-based spectromicroscopic methods to characterize the composition and molecular orientation of the 2SA1PA LB monolayer film. The challenge with this experiment is that the domains of the 2SA1PA system are far too small for PEEM to spatially resolve the phase-structure; therefore other methods were devised in order to characterize the composition and molecular orientation of each domain.

The simplest approach to the problem was to selectively dissolve each domain, and perform spectroscopic measurements on each of them separately. Unfortunately, no procedure was determined which would selectively dissolve the PA domains, as their hydrophobic and lipophobic nature make removal by polar and non-polar solvents difficult. As an alternative approach, the spectrum of the 2SA1PA film was acquired, as well as that for PA after dissolving away the SA domains. The PA signal was then subtracted from the 2SA1PA signal in order to determine the spectrum for SA. To determine whether this method was viable, a major objective to this chapter, the 2SA1PA system was used. The spectrum of 2SA1PA was determined, followed by the spectrum of PA from a 2SA1PA-washed system. The subtraction of the PA spectrum from the 2SA1PA spectrum yielded the spectrum of SA, which compares well with other SA spectra.

To determine if the environment surrounding the system has an effect on the measured spectra, the well-understood system 2AA1PA was used as selective phase dissolution has been used on the system before. Although there were minor differences between samples, the spectrum of the continuous domains in 2AA1PA consisting of PA, pure PA, and PA left from washing the sample were all quite similar. This determined that reliable spectra could be achieved using this method.

Finally, XLDM studies were done on PA, SA, 2SA1PA, and 2SA1PA-washed systems, to determine molecular orientation in these films. The PA system did not exhibit any linear polarization dependence, but PA is a helical molecule, and would not exhibit the same orientation-dependent dichroic features that would be seen in long-chain zig-zag type fatty acid molecules. There was a small decrease in the C-H transition for the pure SA film, therefore exhibiting some polarization dependence. There are too many problems with the percent of polarized light coming from the bending magnet source, as well as the incident angle of the sample in the PEEM microscope, to determine the reason for the polarization dependency of the SA sample.

The 2SA1PA film had different features than the SA film, but exhibited the exact same polarization dependence. This is a somewhat confusing result, as the C1s$\rightarrow\sigma^*_{C\text{-}F}$ peak decreases with the C1s$\rightarrow\sigma^*_{C\text{-}H}$ peak. There was no dependence in the PA sample under the same conditions. Finally, the 2SA1PA washed film demonstrated some radiation damage, but no polarization dependence.

Chapter 3 Exploration of Contrast Mechanisms In PEEM Measurements Using Well-Defined Samples

3.1 Introduction

Energy filtered X-PEEM spectromicroscopy allows the imaging of a sample surface based on photoelectrons of a fixed kinetic. If the incident photon energy is held constant, photoemission image contrast can be varied by changing the selected kinetic energy of the imaging energy analyzer. It is this ability to analyze the distribution of electron kinetic energies (e.g. the spatially resolved photoemission spectrum) that makes it useful in the characterization of novel organic monolayer systems. However, image contrast in energy-filtered PEEM is not well-understood.

Because of the many complex factors that contribute to image contrast in energy-corrected PEEM measurements, it was determined that a better understanding of these complexities would lead to data that is easier to understand. The 2AA1PA system, initially characterized by Qaqish and Paige[15] using AFM, was used for these contrast mechanism experiments. When deposited on a silicon substrate, the 2AA1PA system exhibits the same hexagonal phase-separation as on mica[15], but since silicon is a semiconductor, the sample does not charge in vacuum during the photoemission process. In the following experiments, 2AA1PA films were used to study spatially resolved UPS spectra and the nature of SEEM image contrast for analysis of phase separated LB films.

3.2 Comparisons and Contrast of PEEM and AFM

Atomic force microscopy is an ideal technique for physically characterizing a sample, with high lateral and vertical resolution of its surface topography. There have been many studies where the tip is chemically-modified to yield chemical information on a system, termed chemical force microscopy (CFM)[49], but this is highly dependent on many variables, such as functionalization of the tip and its interaction with surface molecules. As AFM is capable of sub-nanometer vertical resolution, it is therefore used in our studies to characterize and confirm successful

LB deposition. AFM was also used for height measurements, and is responsible for a primary determination of molecular orientation in the domains.

Synchrotron-based NEXAFS X-PEEM experiments are very useful due to the surface sensitivity inherent in photon-in, electron-out spectroscopy techniques[5,8,11,13]. Using PEEM-NEXAFS, spatially-resolved spectra of organic monolayers can be achieved with spectroscopic chemical identification. Therefore, for films such as the mixed fatty acid/perfluorinated fatty acid samples used in these experiments, the C1s$\rightarrow\sigma^*_{C\text{-}H}$ and C1s$\rightarrow\sigma^*_{C\text{-}F}$ transition energy peaks can give a qualitative determination of domain composition. Monitoring the C1s$\rightarrow\pi^*_{C=C}$ transition can also give real time information on the extent of radiation damage.

AFM lacks the chemical sensitivity needed for these experiments, yet is an excellent technique for height and fine structure determination. Synchrotron-based PEEM is excellent at chemical characterization of surface structure. Together they provide substantial information about monolayer film composition, height, and orientation, valence character, and workfunction effects.

3.3 Secondary Electron Emission Microscopy (SEEM)

3.3.1 Contrast Inversion from Secondary Electron Emission Spectroscopy

An important contrast mechanism appears when working with samples exhibiting large workfunctions, such as phase-separated organic monolayers. As the electron kinetic energy used for imaging is varied with the imaging filter, the image contrast depends strongly on differences between the workfunctions of the different phases. The overall image contrast of these phase-separated systems is thus dependent on both the NEXAFS cross-section of the sample material, and on workfunction differences. This is important, as quantitative analysis is then not solely dependent on cross-sectional differences in NEXAFS spectra, but also the imaging electron kinetic energy.

As workfunction can depend on molecular packing and order, differences in the 2SA1PA film domains, versus those of the pure SA and PA films, may be determined using secondary electron emission microscopy (SEEM). Currently

however, 2AA1PA will be used as a model system to determine SE effects, and their application to the study of phase-separated monolayers.

3.3.2 Experimental

As stated above, changes in workfunction occur due to chemical composition differences, and the kinetic energy distribution of secondary electrons can reflect these chemical changes. The domains of systems such as the 2AA1PA phase-separated sample can be differentiated based on the distribution of secondary electron energies. SEEM contrast in the PEEM microscope is due to the electron kinetic energy distribution of the photoelectrons ejected from the sample surface. The sample was mounted into the PEEM experimental chamber. The incident photon energy was set to 62 eV, and the sample, objective lens voltage, sample tilt, and sample distance to objective lens were adjusted to bring the sample into focus. Once in focus, the electron kinetic energy was varied from -2 eV to +3 eV. The resulting changes in contrast were observed, as three-dimensional stacks (x, y, energy) with 0.2 eV steps and 150 ms dwell averaged twice.

3.3.3 Results and Discussion

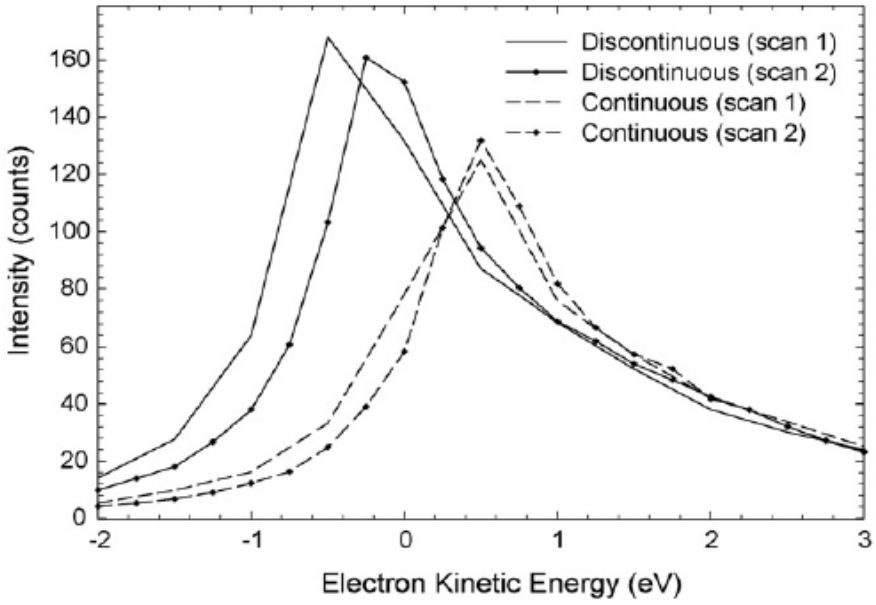

Figure 3.1 - Secondary electron photoemission spectra of 2AA1PA, showing differences in kinetic energy distribution in the PA phase (continuous), and the AA phase (discontinuous). Incident photon energy was 62 eV.

Figure 3.1 shows the change in the kinetic energy distribution of the secondary electron peak. Notice the PA region (continuous) is shifted to higher kinetic energy, while the AA domain contribution (discontinuous) is shifted to a lower kinetic energy. This is due to the greater binding energy of the carbon core electron when coordinated to a more electronegative species, such as fluorine. The shift to lower energy for the AA phase is due to lower energy requirements for the removal of an electron from a C-H bound carbon, than that of a C-F bound carbon.

The 2AA1PA system (figure 3.2), demonstrates the effect of workfunction-based control of the contrast as the electron kinetic energy is scanned through 1.5 V.

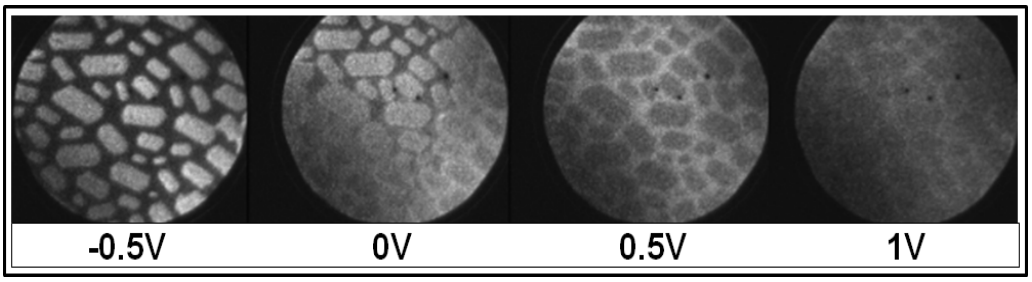

Figure 3.2 - SEEM of 2AA1PA LB film on silicon substrate (hν = 695 eV) demonstrating contrast inversion.

Section 4.2.1 will describe an observed domain sized effect, the origin of which has yet to be determined. As the electron kinetic energy is scanned from a low to a high energy distribution of photoelectron kinetic energies, the 2AA1PA domains appeared to grow in size. This effect was not always reproducible, and its cause is still of interest. The effect may be a real effect, or may be due to radiation damage. It is speculated that the effect is due in some part to the interface between the AA discontinuous and PA continuous domains.

3.4 Ultraviolet Photoelectron Spectroscopy (UPS)

Discussed in section 1.5.1, UPS is the photoelectron spectroscopy of the valence band using ultraviolet light. The ability to do UPS spectromicroscopy of organic thin film systems, while sustaining little radiation damage would be very useful for material studies. Currently UPS spectromicroscopy of these systems is hindered by the susceptibility of organic monolayers to radiation damage, and the long dwell times or high flux required to collect spectra of adequate signal to noise.

In this section, UPS is used in two experiments separate experiments. The first is the acquisition of UPS spectra in "image sequence mode" on the PGM beamline. The second is the acquisition of UPS spectra in "dispersion mode" on the SM beamline. "Dispersion mode" is the direct imaging of dispersion plane of the hemispherical analyzer yielding a ~10eV range of the spectrum in a single image.

3.4.1 Selection of Optimal UPS Photon Energy

As noted previously, a 2AA1PA sample was prepared on silicon and placed in the CaPeRS PEEM on the PGM beamline at the CLS. Initial experiments were conducted to determine what was achievable on the PEEM microscope, and the initial problems to be overcome. UV experiments were initially performed at 21.2 eV and 40.8 eV, as comparison of spectra could then be made with spectra from non-synchrotron experiments (He Iα and He IIα energies). It was necessary to change the monochromator energy grating on the PGM beamline, as the most flux at 21.2 eV comes from using low-energy grating, while there are more 40.8 eV photons using the medium energy grating.

A difficulty encountered with these energies is that when the incident photon energy is low, the valence photoemission features overlap with the secondary electron (SE) peak. A lack of valence orbital features meant that the incident energy needed to be increased until the SE peak no longer obscur the spectral features of interest. A higher photon energy (62 eV), was used to separate the primary photoemission peaks from the secondary electron band. These experiments were conducted using a 20 μm field of view, with 0.5 eV steps and no contrast aperture to increase signal.

3.4.2 Image Sequence UPS on PGM Beamline

3.4.2.1 Experimental Determination of Domain-Specific UPS Spectra

Once it was decided that a 62.0 eV photon energy was appropriate for UPS experiments, spectromicroscopy of the 2AA1PA system was attempted. Long dwell times and averaging were needed to produce images with good contrast. The procedure was therefore modified to provide image contrast for the aXis2000 software to extract domain-specific information with low radiation damage. To acquire low-dose UPS of the 2AA1PA system, the beam was shuttered, and the sample moved so that a fresh area was available. The multichannel plate (MCP) was set to a maximum value of 1450 V with the 50 μm x 50 μm slits set on the beamline and the 500 ms dwell averaged twice.

When ready, the shutter was removed, and a stack of images (x, y, energy) was acquired from 30 eV-60 eV electron kinetic energies with 0.5 eV steps at

incident photon energy of 62 eV. The MCP was then turned down to 1318 V, and the electron kinetic energy set at 0 V. The shutter was again removed, and an image was taken using 1500 ms dwell averaged by 10. Using this method, each area is used for a low-dose UPS stack, followed by a high-contrast image of the same area. This procedure was repeated many times in order to average the spectra and achieve better low-dose UPS statistics. Using the aXis2000 software package, masks were made from the high-contrast images, and then applied to the image stacks. In this manner, domain-specific spectra can be acquired with minimal radiation damage.

Qaqish and Paige have determined that, although the molecules in solution and on the air-water interface phase-separate, they do not completely phase-separate, with up to 17% AA in the continuous domain for the 2AA1PA system[15]. It is theorized that this mixing has an effect on the overall molecular orbital energies via intermolecular interactions.

3.4.2.2 Results and Discussion of UPS Spectral Differences

Figure 3.3 shows the UPS spectra of a pure AA sample, a pure PA sample, and the discontinuous (AA) and continuous (PA) regions of the phase-separated 2AA1PA sample.

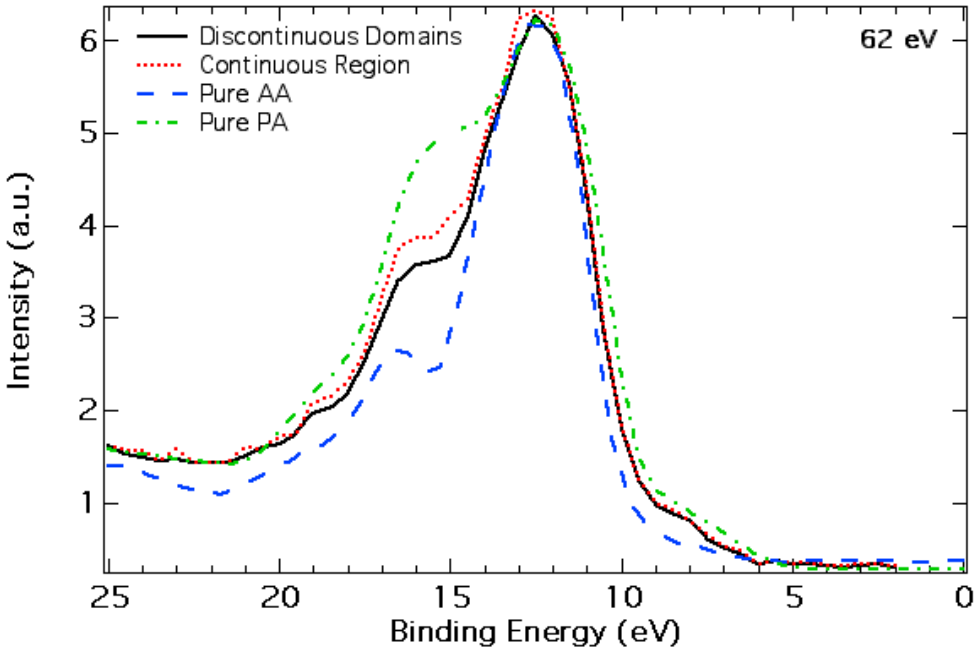

Figure 3.3 - UPS spectra of 2AA1PA film discontinuous and continuous domains, as well as AA and PA spectra. The spectra were taken at 62 eV, and are energy shifted to the maxima for comparison.

The photoemission spectra of the discontinuous and continuous regions of the 2AA1PA film are similar, although there is a greater contribution to the peak at 16 eV from the continuous region, than that from the discontinuous domains. This peak is also present in the PA and AA samples, although shifted to a slightly higher binding energy of 16.5 eV. The reason the spectra were shifted on the energy scale, is that tilt and the energy-filter have a major effect on the energy scale of the spectra, and because of this the energies are not taken as absolute energy values.

The substantial differences in the PA and AA phases in comparison to their phase-separated counterparts, as well as the intensity of the discontinuous and continuous regions falling midway between those of the PA and AA, led to the suggestion that valence energy mixing might occur with mixing of phase components. Valence mixing occurs when valence orbitals of similar energies interact, resulting in the lowering or increasing of valence energies in the affected molecules. The similarity in the discontinuous and continuous domains suggests domain-based valence character mixing is occurring.

As radiation damage is a problem with monolayer organic systems, the contrast aperture was removed from the microscope path. This is a compromise, because while it improves the radiation damage problem, it allows signal from outside the selected region of interest to "seep-in" to the measurement. This may be another strong reason why the discontinuous and continuous phase UPS spectra are so similar, as signal from each domain may have introduced itself into the measurements of the other domain. The contrast aperture is therefore necessary, but only useful when there is a sufficiently large signal and reducing the transmission of the analyzer is not too detrimental to the experiment.

The gain in removing the contrast aperture is that there is more signal available for the experiment. For the UPS spectra in figure 3.3, there would be nearly no signal if the contrast aperture were not removed. Therefore the decision is to run an experiment with degradation, or not run the experiment. Radiation damage and the halo effect provide a limit to the use of UPS-PEEM for ultra-thin films.

3.4.2.3 Radiation Damage of 2AA1PA System Experiment

To determine how resistant the 2AA1PA system is to low-dose UPS radiation, 30 minute scans were run from 30 eV to 60 eV at an incident photon energy of 62 eV. A series of scans were run to explore changes with radiation dose. Large 0.5 eV steps were used; with a 2000 ms dwell time, no averaging, and 50 μm x 50 μm slits. The subsequent SEEM image reduced the MCP to 1318 V so as to not damage the CCD camera, and the electron kinetic energy to 0 V. Image dwell was 1500 ms, averaged 10 times. Masking techniques were again used to determine radiation damage sensitivity for the discontinuous and continuous phases.

3.4.2.4 Radiation Damage of 2AA1PA System Results and Discussion

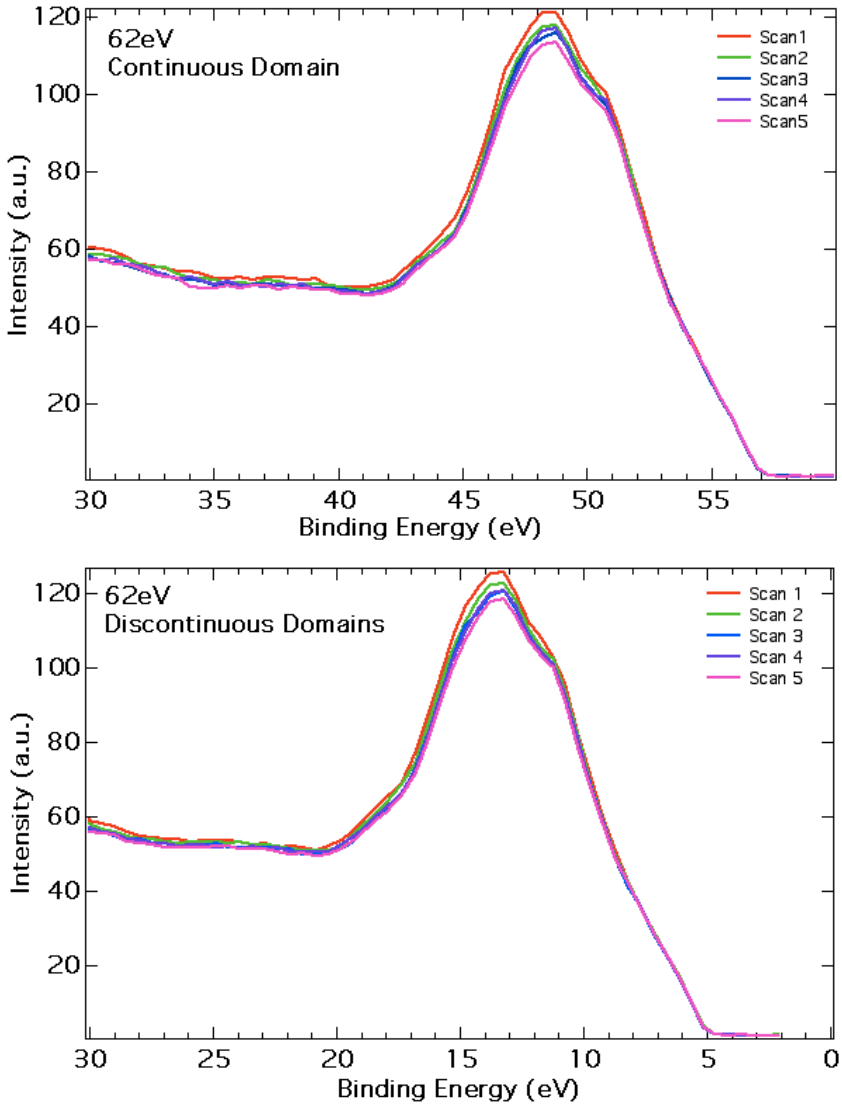

Figure 3.4 - UPS of continuous and discontinuous 2AA1PA domains (consecutive scans taken over 25 minutes).

As evident in figure 3.4, there is little change to the spectra as a function of radiation exposure (~ 8% decrease in continuous domain at 11.5 eV, 5% decrease in discontinuous domain at 13.5 eV). The small change to the spectra with exposure indicates that, under the scanning conditions used, radiation damage is either very slow (figure 3.4), or the radiation damage is extremely quick and relatively complete

before the first low-dose scan is finished. This is one of the driving reasons behind using dispersion mode to obtain UPS spectra (discussed in section 3.5).

3.4.2.5 Radiation Damage of Pure AA System Experiment

The differences in the UPS spectra between the pure film systems (AA and PA) and the 2AA1PA mixed-phase systems (continuous and discontinuous phases) were shown to be quite significant in figure 3.5 (section 3.4.2.6). Determining if there is radiation damage using the same method as the 2AA1PA system gave insight into how significant the valence character mixing effect is, as well as determining if the radiation damage occurs slowly or too rapidly to measure.

3.4.2.6 Radiation Damage of Pure AA System Results and Discussion

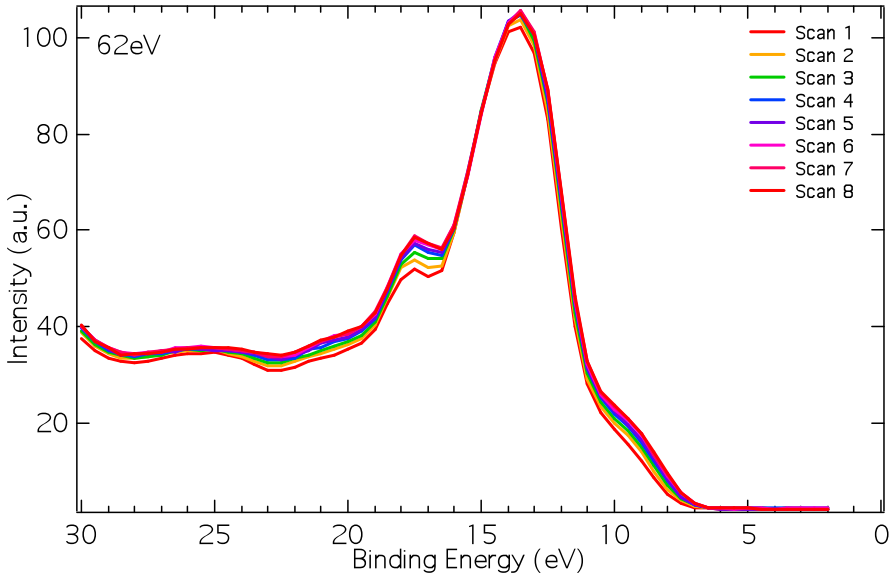

Figure 3.5 - UPS of pure AA sample (consecutive scans taken over 25 minutes).

Figure 3.5 shows that there is very little change due to radiation damage of pure AA over a 25 minute period. Over this time period, the peak at 17.5 eV grows in intensity by ~16%. As it was uncertain how fast the AA and PA films were damaged by radiation, this experiment was conducted to determine if the differences in spectra being observed (figure 3.5) were of the phases before or after radiation

damage. This experiment, along with the following section 3.9, was conducted to determine the extent of radiation damage with respect to time. As it is only the feature at 17.5 eV which is appreciably affected by radiation damage, it can be concluded that radiation damage, at least in part, occurs on the order of minutes. There may still be significant radiation damage occurring too quickly to notice, and as mentioned previously, the relatively fast acquisition times of UPS spectra in dispersion mode has the potential to capture this information.

3.4.2.7 Radiation Damage of Pure PA System: Experiment

As with the AA system, determining the extent of radiation damage to the film enabled a more thorough understanding of radiation damage in the PA system. The experiment was conducted in the exact same manner as the PA system in section 3.8, over a 25 minute time period. The scans were then compared to see the effect of radiation damage on the system.

3.4.2.8 Radiation Damage for Pure PA System: Results and Discussion

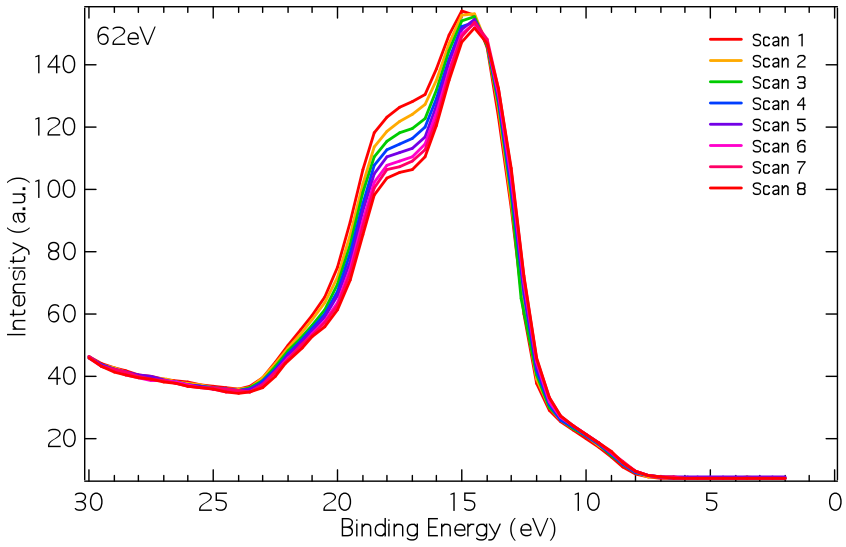

Figure 3.6 - UPS of pure PA sample (consecutive scans taken over 25 minutes).

Figure 3.6, like the AA UPS data, suggests that some radiation damage occurs slowly at valence energies, as the decrease in the 17.5 eV peak (~13%) occurs slowly

over 25 minutes of continuous irradiation. This result again does not rule out that some radiation damage is occurring rapidly before the first scan, and this will be determined in future experiments.

3.5 Low-Dose Dispersion-Mode UPS Studies

3.5.1 Tilt in Low-Dose UPS Experiments

Sample tilt can have a large influence on contrast in organic films, and this effect is amplified on energy-filtered PEEM imaging devices such as the CaPeRS microscope. As noted in section 2.7, when the sample plane is not normal to the objective lens, changes to the electric field change the distribution of kinetic energies photo-ejected from the surface, and therefore change the energies of electrons accepted by the analyzer.

Though this does not seem like a significant problem if the sample is mounted without tilt, it is very difficult to accomplish this. A caliper was used to minimize tilt by ensuring the sample was equidistant from the sample holder on each side, but this method does not work perfectly. Small changes in sample tilt affect the electric field of the sample. The greater the tilt, the more difficult it is to maintain focus as different areas of the sample are scanned. As the sample is moved from where it was originally focused, the sample changes z-position to the objective lens and focus is lost.

When low-dose experiments are performed, multiple scans are often carried out so that they can be averaged, but the experimenter must continuously adjust the tilt between each scan. This means that there will be intensity differences between each scan, and direct comparison between scans is difficult. It is essential to mount the sample with as little tilt as possible, so as to minimize radiation damage.

3.5.2 Dispersion Mode Experiment

Dispersion mode is a method useful in reducing radiation damage incurred during long UPS scans. As samples are damaged by excess ionizing radiation, the PEEM now has the ability to take a few short scans and get SE or UPS spectra with minimal damage.

There are advantages and disadvantages to using dispersion mode on phase-separated organic monolayers. An advantage to dispersion mode studies is the very fast acquisition time of each scan. By adjusting the energy analyzer exit slits to allow a strip of ~10 eV, the UPS or SE spectra can be obtained with a dwell of only ~100 ms. With some overlap, a UPS or SE spectrum over a 20 eV range can be acquired, with little more than three or four scans. This extra time added to the estimate depends on the speed at which desired domains can be found for analysis.

Thus far, the procedure consists of setting the field of view to 8 μm and inserting the second contrast aperture, adjusting for the best image in an already damaged area of the sample. Once aligned, the film is then moved to an undamaged region where the AA domain fills the entire field of view, and the beamline shutter is closed. The MCP is reduced and dispersion plane mode is enabled. The MCP must be reduced, as selecting dispersion plane mode focuses the beam, and could damage the CCD camera if too bright. The shutter is opened, the lenses adjusted to focus the beam to as sharp a line as possible, and the shutter is closed again. When ready, the shutter is again opened; the SE spectrum in dispersion mode is taken at the selected electron kinetic energy. The final step may be repeated at various energies for a larger energy range. Figure 3.7 below demonstrates three such scans of the secondary electron peak in dispersion mode. The 0 V spectrum exhibits the electron energy band displaced to a lower energy, while the 10 V spectrum exhibits displacement of the band to a higher energy.

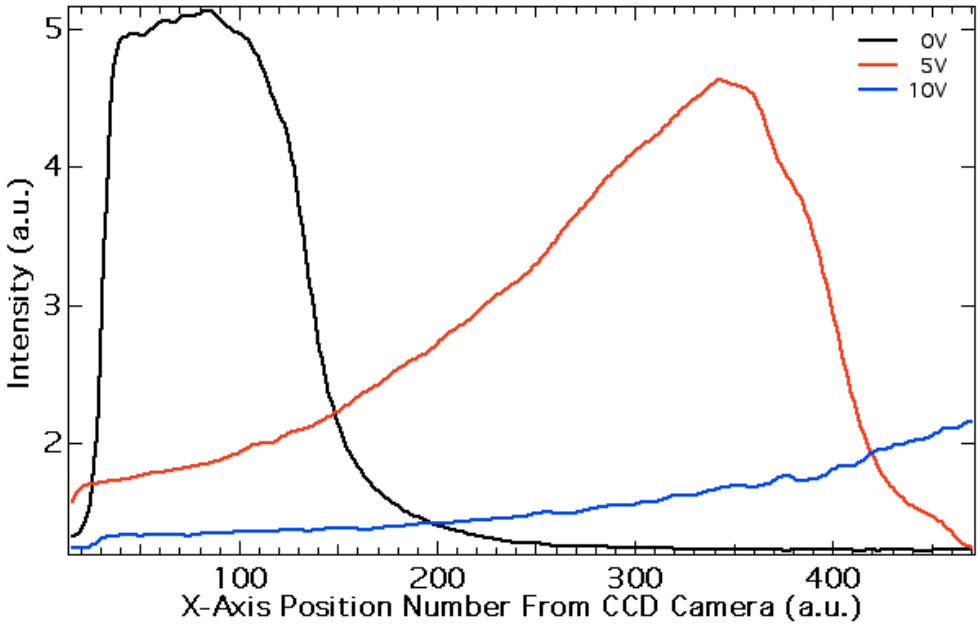

Figure 3.7 - Graph of 2AA1PA secondary electron photoemission spectra with electron kinetic energy at 0 V, 5 V, and 10 V. Spectra 5-point smoothed.

Figure 3.8 below is the secondary electron photoemission spectra of pure AA and pure PA films. Variation in energy scale and intensity due to sample tilt and radiation damage induced workfunction change due to photodesorption yields results which are difficult to interpret. There is a significant difference in the secondary electron photoemission spectrum of the AA and PA domains, however the origin of the feature difference is difficult to determine.

Due to the unpredictable energy scale (an instrument specific variable), and radiation damage (intrinsic in the data acquisition process), this technique does not work well for thin film organic systems.

The spectra below have been aligned so as to be comparable; however, the lack of a proper energy scale renders arbitrary energy values. Tilt in the sample, as well as desorption of water from the film, produce instability in an already problematic energy scale.

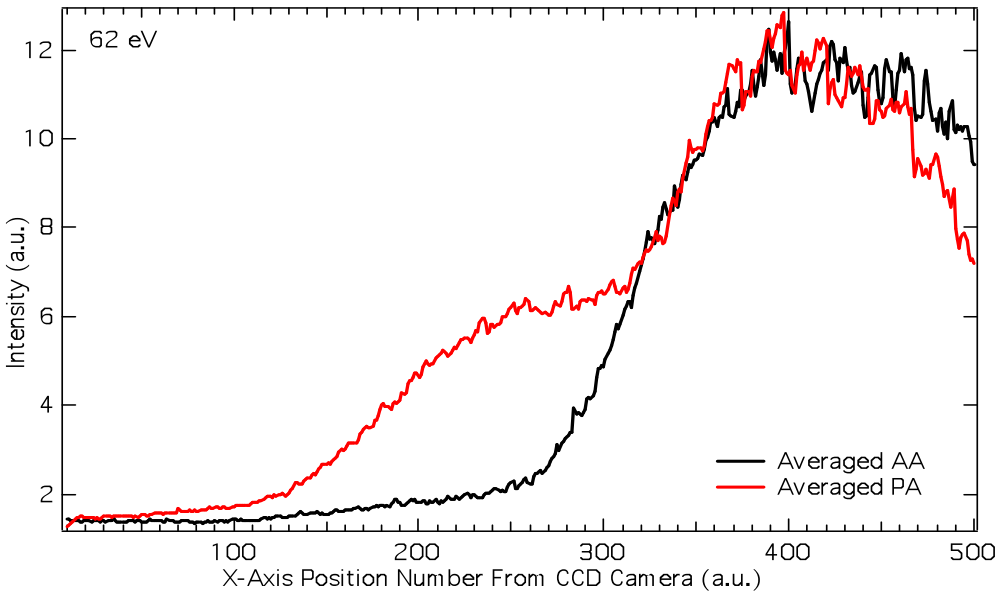

Figure 3.8 – Graph of AA and PA secondary electron photoemission spectra with electron kinetic energy of 0 V.

3.5.3 Dispersion Mode Results and Discussion

A major disadvantage of this method is evident when the UPS or SE spectra of individual domains in a phase-separated sample are desired. As this is purely a spectroscopic technique, the desired domain must first be located using SEEM, and fill the entire field of view. This is a difficult experiment, as locating the domain quickly before too much radiation damage requires experience. Dr. Uday Lanke's expertise was invaluable in this endeavor.

The minimum field of view capable for these experiments was 8 μm, and while the temperature of the 2AA1PA LB system and the aggregation and Otswald Ripening mechanisms described by Qaqish and Paige[19] were allowed time to increase the size of the AA domains, the continuous region was still visible as the AA domains were never larger than the 8 μm field of view. This project is discussed in further detail in section 4.2.2.

3.6 Summary

There are many mechanisms that effect image contrast on a PEEM. One of the major goals of this project was to use a well-defined phase-separated organic LB monolayer to better understand PEEM contrast mechanisms involved with UPS and SEEM. This chapter compared contrast in the PEEM via workfunction, with that provided by the atomic force microscope.

Contrast was also discussed in terms of workfunction effect. If the kinetic energy of the incident photon is greater than the work function of the sample, the electron has enough energy to escape into the continuum. If the energy of the incident photon is less than the workfunction, the electron does not have enough energy to escape into the continuum and there is no photoemission. This is the reason that, although the PA continuous domain in the 2AA1PA sample brightens when its ionization energy is reached, it remains darker than the discontinuous AA domains the entire time. This workfunction effect is also the reason that, when the band-pass of allowed secondary electron kinetic energies is scanned, the distribution admitted will affect the contrast, and can cause contrast inversion.

Secondary electron emission microscopy (SEEM) was discussed, and described in more detail the factors leading to, and effects of, contrast inversion. The SE photoemission spectra of 2AA1PA were described, and demonstrated that the kinetic energy distribution of secondary electrons is different dependent on the workfunction of the sample, or more understandably, dependent on the composition of the sample region of interest.

UPS was used extensively on the 2AA1PA film, along with pure AA and pure PA. Scans were taken on the PGM beamline using this method, and the incident energy was determined to be 62 eV, as the He Iα and He IIα energies were too convoluted and suppressed by the strong secondary electron peak.

The UPS spectra of the discontinuous and continuous phases of the 2AA1PA film, as well as the pure AA and pure PA samples, were compared and determined to yield different results. There results needed to be rescaled to each other, as tilt and the energy-filter affect the energy distribution of electrons photo-ejecting from the sample.

All samples were submitted to radiation damage studies, to determine if that would affect contrast. The continuous and discontinuous domains of the 2AA1PA sample were found to exhibit little long-term (> 5 minutes) radiation damage, although future experiments using dispersion mode will allow short-term (< 5 minutes) radiation damage determination. The UPS of AA showed radiation damage in a comparable timeframe to the PA, but the peak at 17.5 eV was increasing with radiation damage in the AA, while decreasing with radiation damage in the PA. Future studies would be interesting to include short-term dispersion mode studies, as well as much longer radiation damage studies.

Chapter 4 Conclusions and Future Work

4.1 Conclusions

As discussed in chapter 1, the purpose of this M.Sc. project was to both gain a better understanding of PEEM-based contrast mechanisms, through experimentation with a well-known LB monolayer system (2AA1PA), and use established PEEM-based techniques to characterize a lesser-known sample (2SA1PA).

4.1.1 Application of Well-Understood PEEM-Based Measurements for Characterization of New Samples

As for the application of well-understood PEEM-based measurements for characterization of new samples, the project demonstrated the power of this technique, even when used as only a spectroscopy tool. As interest in phase-separated LB monolayers continues to be strong, the chemical characterization of domains remains a difficult task. With increased access to PEEM-based methods, and better-understood and easier to use systems, PEEM has the potential of becoming more and more common in organic surface science.

In this project, the chemical characterization of a phase-separated LB monolayer, 2SA1PA, was determined using a modified NEXAFS technique. This technique, whereby the spectrum of one phase is subtracted from the spectrum of the entire sample, yielded the spectrum of the other domain. The analysis of subtraction method data is problematic, as changes in intensity occur as many variables (ring current, tilt, etc.) contribute to signal intensity, resulting in a technique that is purely qualitative and prone to creating spectrum artifacts. Other problems that affect the characterization of this film were the low signal, as it is a monolayer and SA seems to be lying on the surface and therefore there is not a large quantity of material to sample.

Determination of molecular orientation is still a work in progress. Though some orientation data was acquired, the reduced linear polarization of the 7.3.1.1 bending magnet at the ALS (~80% linear polarization), as well as the 30° incident angle of the PEEM-2, mean that better measurements are possible.

In the end, the SA and PA domains were identified, and therefore a large portion of this goal was completed.

4.1.2 Exploration of Contrast Mechanisms in PEEM-Based Measurements Using Well-Defined Samples

Well-characterized 2AA1PA samples were used to better understand the contrast mechanisms inherent in PEEM. As there are many different contrast mechanisms available to the PEEM, determining which are most affected by changes in the microscope is necessary. The determination that in organic systems, workfunction contrast can have as great an effect as photoabsorption cross-section contrast is important. It was determined that small changes to the electron kinetic energy parameter on the PEEM can affect the secondary electron peak, shifting the kinetic energy distribution of the ejected electrons significantly. Studies were carried out using SEEM to better understand PEEM-based contrast mechanisms. SEEM determined PEEM contrast can depend largely on the workfunction of organic materials.

UPS experiments demonstrated that there is some long-term radiation damage apparent in the UPS spectra, as well as providing insight that supports the mixing of valence character, as the domains for continuous and discontinuous phases in 2AA1PA were different than those taken from pure samples. The study also determined how greatly sample tilt can affect the electric field coming off the sample holder, skewing results, and changing the kinetic energy distribution.

4.2 Future Work

4.2.1 SEEM Domain Size

A curiosity in the SEEM experiments involving the 2AA1PA mixed-phase system was that the domain size seemed to increase as the relative kinetic energy of the secondary electrons increased. Figure 4.1 shows this effect. It would be interesting to determine whether this effect is a domain interface effect due to radiation damage, or due to a difference in secondary emission of the interface.

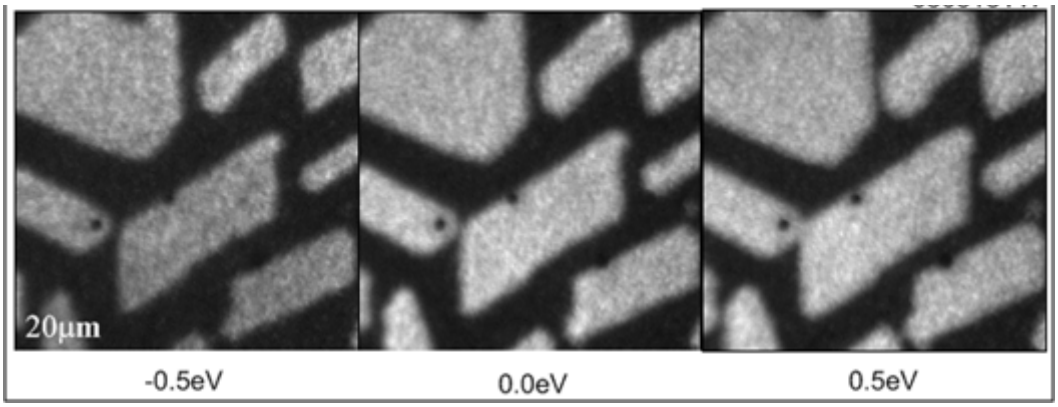

Figure 4.1 - 2AA1PA SEEM images showing an increase in domain size with increase in kinetic energy distribution of the secondary electrons.

This effect was observed when there were other priority projects, and time could not be spared to explore it further. To determine whether this is radiation damage, an interface effect, or analyzer artifact, the experiment should be reproduced while scanning to lower kinetic energies. If the domains continue to grow than the effect is due to radiation damage, if they shrink, it may be due to an interface effect, or analyzer artifact.

4.2.2 Dispersion Mode

As these experiments were commenced very near the end of this project, the utility of this method has not yet been ascertained. Initial SE measurements in dispersion mode were run on the SM beamline in March 2009. The purpose of this initial study was to first determine if the spectra could be obtained of the secondary electron emission peak. When this was successful dispersion mode UPS was attempted, but no results were obtained. It was decided to work on streamlining the dispersion mode SE acquisition procedure before continuing with dispersion mode UPS.

Future experiments should be conducted on pure samples so as to determine the effectiveness of the technique with a simple system before using the more complex phase-separated 2AA1PA system. When a more complex system is needed, instead of 2AA1PA, a higher ratio system should be used, such as 3AA1PA or 4AA1PA so as to ensure domains are large enough to fill entire field of view. The

converse can be done if the previous experiment is successful, in that the ratio is decreased to 1AA3PA or 1AA4PA so as to increase the size of the continuous phase and obtain SE and UPS information for the continuous domain.

New radiation studies should be conducted, due to the lack of data on fast radiation damage. Previous UPS experiments have determined that there is some long-term radiation damage, but there is interest is what occurs immediately upon irradiation. If radiation damage occurs too quickly, as is thought to be the case, it may be possible to detune the undulator on the SM beamline to reduce the beam intensity by hindering its ability to collimate photons.

As some radiation damage studies were conducted over a period of less than 30 minutes, it is also of interest to determine the extent of damage over longer time intervals. Monitoring the extent of radiation damage over a longer period would provide a better understanding as to the extent of long-term beam damage.

4.2.3 XLDM of 2AA1PA, 2SA1PA, and Pure PA Using F1s-edge

F 1s experiments on the SM beamline, with its ability to create nearly 100% linear polarized light, together with the shallow incidence angle of the CaPeRS X-PEEM, would greatly help in determining the orientation of the 2AA1PA, 2SA1PA, and PA films.

The Ziegler et al. experiments[18], discussed in section 2.11.2, demonstrate the ability to determine linear dichroism dependence using the F1s spectra of the system, and while this experiment hasn't been performed yet, it shows promise. The PA signals for the 2AA1PA, 2SA1PA, and pure PA systems are very strong, and have very intense features. Figure 4.2 is an over-plot of the F1s spectrum from the continuous domain of the 2AA1PA system with the Ziegler data[18]. This initial data suggest that the PA molecules are oriented somewhere between 67.5° and 90° to the substrate surface, suggesting these experiments could determine the molecular orientation of the PA phase in 2SA1PA, as well as compare the orientations of PA in the 2AA1PA, 2SA1PA, and pure PA samples.

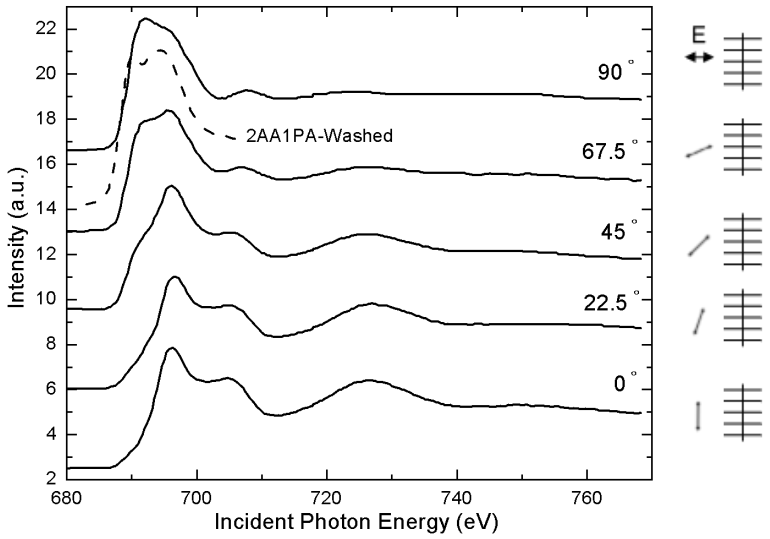

Figure 4.2 - F1s NEXAFS spectrum of 2AA1PA continuous phase (dotted black) in comparison with data from Ziegler et al.[18] to determine molecular orientation and existence of domain anisotropy. (Figure adapted from Ziegler et al., 1994)

Doing experiments at the F 1s edge has the added advantage of not having to contend with carbon contamination of the beamline optics upstream of the endstation (decrease of signal at C K-edge is referred to as the 'carbon dip'). Theoretically this means that normalization will be a more simple process and there will be far less contamination. A problem with this is that the sample will become even more radiation sensitive if the incident photons are at the F 1s edge. Because of its electronegativity, fluorine is very easily removed from samples.

4.2.4 XLDM of 2AA1PA, 2SA1PA, AA, SA, and PA on SM Beamline

As the CaPeRS PEEM is now a permanent fixture on the SM beamline, it provides a perfect opportunity to use C1s NEXAFS for molecular order determination. The near-100% linearly polarized light, together with a more shallow incident photon angle of the PEEM will enable more efficient data acquisition. The shutter will minimize the radiation damage problem, as would a slightly detuned undulator. The ability to minimize the length of the acquisition time by exposing the sample to the beam for only a brief moment between energy steps, would reduce

radiation damage. Although there may not be any definitive changes in the C1s→$\sigma^*_{C\text{-}F}$ transition, there should be no reason that polarization dependent changes, such as the C1s→$\sigma^*_{C\text{-}H}$ and C1s→$\sigma^*_{C\text{-}C}$ transitions, would not be observed.

4.2.5 SEEM Radiation Study

As the sample is being bombarded by radiation, loosely-bound or physisorbed molecules (i.e. water) will desorb from the sample surface. The desorption of these surface molecules affects the workfunction of the sample. As SEEM is sensitive to workfunction, the observed distribution of electron kinetic energies from the surface affects the secondary electron photoemission spectrum.

There have been a few internal studies about SEEM radiation damage, and if the shift in workfunction contrast is affected, it would be interesting to note the magnitude of this effect. This can be done with any film, but for simplicity the more understood 2AA1PA should be used.

References

1. M. Matsumoto, K. Tanaka, R. Azumi, Y. Kondo and N. Yoshino, Langmuir, 19 (2003) 2802.

2. R. Overney, E. Meyer, J. Frommer, H. Güntherodt, M. Fujihira, H. Takano and Y. Gotoh, Langmuir, 10 (1994) 1281.

3. L. Matos, J.-C. Ravey and G. Serratrice, Journal of Colloid and Interface Science, 128 (1989) 341.

4. R. Overney, E. Meyer, J. Frommer, D. Brodbeck, R. Luthi, L. Howard, H.J. Guntherodt, M. Fujihira, H. Takano and Y. Gotoh, Nature, 359 (1992) 133.

5. P. Hale, S. Turgeon, P. Horny, F. Lewis, N. Brack, G. Van Riessen, P. Pigram and D. Mantovan, Langmuir, 24 (2008) 7897.

6. M.C. Petty, Langmuir-Blodgett Films, Cambridge University Press, Cambridge, 1996.

7. A. Ulman, An Introduction To Ultrathin Organic Films From Langmuir-Blodgett to Self-Assembly, Academic Press, Inc., Toronto, 1991.

8. M. Przychowski, G. Marx, G. Fecher and G. Schönhense, Surface Science, 549 (2004) 37.

9. A. Hitchcock, C. Morin, X. Zhang, T. Araki, J. Dynes, H. Stöver, J. Brash, J. Lawrence and G. Leppard, Journal of Electron Spectroscopy and Related Phenomena, 144 (2005) 259.

10. A.D. Smith, P.F. Schofield, A. Scholl, R.A.D. Pattrick and J.C. Bridges, Journal de Physique IV, 104 (2003) 373.

11. S. Christensen, U.D. Lanke, B. Haines, S.E. Qaqish, M.F. Paige and S.G. Urquhart, Journal of Electron Spectroscopy and Related Phenomena, 162 (2008) 107.

12. O. Benka and P. Zeppenfeld, Journal of Physics: Condensed Matter, 17 (2005) S1311.

13. A. Cossy-Favre, J. Diaz, Y. Liu, H. Brown, M. Samant, J. Stohr, A. Hanna, S. Anders and T. Russells, Macromolecules, 31 (1998) 4957.

14. C.M. Schneider, Soft X-Ray Photoelectron Emission Microscopy (X-PEEM), in F. Hippert (Eds), Neutron and X-Ray Spectroscopy, Springer, Netherlands, 2006.

15. S. Qaqish and M. Paige, Langmuir, 23 (2007) 2582.

16. H. Takano, J.R. Kenseth, S.S. Wong, J.C. O'Brien and M.D. Porter, Chemical Reviews, 99 (1999) 2845.

17. J. Fu and S. Urquhart, Journal of Physical Chemistry A, 109 (2005) 11724.

18. C. Ziegler, T. Schedelniedrig, G. Beamson, D.T. Clark, W.R. Salaneck, H. Sotobayashi and A.M. Bradshaw, Langmuir, 10 (1994) 4399.

19. S.E. Qaqish and M.F. Paige, Langmuir, 24 (2008) 6146.

20. M. Krafft and M. Goldmann, Current Opinion in Colloid & Interface Science, 8 (2003) 243.

21. S. Jang, M. Blanco, W. Goddard, G. Caldwell and R. Ross, Macromolecules, 36 (2003) 5331.

22. D.A. Siber., http://www.nanotech-now.com/Art_Gallery/antonio-siber.htm, 2003; (accessed 2008).

23. Y.F. Hu, L. Zuin, R. Reininger and T.K. Sham, AIP Conference Proceedings, 879 (2007) 535.

24. K.V. Kaznatcheev, C. Karunakaran, U.D. Lanke, S.G. Urquhart, M. Obst and A.P. Hitchcock, Nuclear Instruments and Methods in Physics Research Section A: Accelerators, Spectrometers, Detectors and Associated Equipment, 582 (2007) 96.

25. S. Anders, H. Padmore, R. Duarte, T. Renner, T. Stammler, A. Scholl, M. Scheinfein, J. Stöhr, L. Séve and B. Sinkovic, Review of Scientific Instruments, 70 (1999) 3973.

26. E. Bauer, Journal of Electron Spectroscopy and Related Phenomena, 114 (2001) 975.

27. J. Genzer, E.J. Kramer and D.A. Fischer, Journal of Applied Physics, 92 (2002) 7070.

28. L. Gregoratti, T. Mentes, A. Locatelli and M. Kiskinova, Journal of Electron Spectroscopy and Related Phenomena, 170 (2009) 13.

29. J. Als-Nielsen and D. McMorrow, Elements of Modern X-Ray Physics, John Wiley & Sons, Ltd., Toronto, 2001.

30. J. Stohr, NEXAFS Spectroscopy, Springer, New York, 2003.

31. O. Dhez, H. Ade and S. Urquhart, Journal of Electron Spectroscopy and Related Phenomena, 128 (2003) 85.

32. L. Gamble, B. Ravel, D. Fischer and D. Castner, Langmuir, 18 (2002) 2183.

33. S. Hufner, Photoelectron Spectroscopy, Springer, New York, 2003.

34. J.H.D. Eland, Photoelectron Spectroscopy, Butterworths & Co. Publishers, 1984.

35. N. Ueno, K. Sugita, K. Seki and H. Inokuchi, Physical Review B, 34 (1986) 6386.

36. J.B. Hudson, Surface Science, Butterworth-Heinemann, Stoneham, MA, 1992.

37. K.V. Kaznacheyev, C. Karunakaran, F. He, M. Sigrist, T. Summers, M. Obst and A.P. Hitchcock. Journal 2007; 582: 103.

38. Y.F. Hu, L. Zuin, G. Wright, R. Igarashi, M. McKibben, T. Wilson, S.Y. Chen, T. Johnson, D. Maxwell, B.W. Yates, T.K. Sham and R. Reininger, Review of Scientific Instruments, 78
(2007) 083109.

39. T. Stammler, S. Anders, H. Padmore, J. Stohr, M. Scheinfein and H. Ade, Materials Research Society Symposia Proceedings, 524 (1998) 25.

40. B. Frazer, M. Girasole, L. Wiese, T. Franz and G. Stasio, Ultramicroscopy, 99 (2004) 87.

41. D. Outka, J. Stohr, J. Rabe and J. Swalen, Journal of Chemical Physics, 88 (1988) 4076.

42. D. Outka, J. Stöhr, J. Rabe, J. Swalen and H. Rotermund, Physical Review Letters, 59 (1987) 1321.

43. J. Stöhr, Y. Wu, B. Hermsmeier, M. Samant, G. Harp, S. Koranda, D. Dunham and B. Tonner, Science, 259 (1993) 658.

44. A. Fujimori, Y. Sugita, H. Nakahara, E. Ito, M. Hara, N. Matsuie, K. Kanai, Y. Ouchi and K. Seki, Chemical Physics Letters, 387 (2004) 345.

45. J. Wang, C. Morin, L. Li, A. Hitchcock, A. Scholl and A. Doran, Journal of Electron Spectroscopy and Related Phenomena, 170 (2009) 25.

46. B.H. Frazer, B. Gilbert, B.R. Sonderegger and G. De Stasio, Surface Science, 537 (2003) 161.

47. B.L. Henke, E.M. Gullikson and J.C. Davis, Atomic Data and Nuclear Data Tables, 54 (1993) 181.

48. W. Luzny, E.J. Samuelsen and D.W. Breiby, Synthetic Metals, 119 (2001) 203.

49. G. Chen, X. Ning, B. Park, G. Boons and B. Xu, Langmuir, 5 (2009) 2860.